The Role of Bottom Vortex Stretching on the Path of the North Atlantic Western Boundary Current and on the Northern Recirculation Gyre

RONG ZHANG

Geophysical Fluid Dynamics Laboratory, National Oceanic and Atmospheric Administration, Princeton, New Jersey

GEOFFREY K. VALLIS

Geophysical Fluid Dynamics Laboratory/Atmospheric and Oceanic Sciences Program, Princeton University, Princeton, New Jersey

(Manuscript received 20 June 2005, in final form 24 October 2006)

ABSTRACT

The mechanisms affecting the path of the depth-integrated North Atlantic western boundary current and the formation of the northern recirculation gyre are investigated using a hierarchy of models, namely, a robust diagnostic model, a prognostic model using a global 1° ocean general circulation model coupled to a two-dimensional atmospheric energy balance model with a hydrological cycle, a simple numerical barotropic model, and an analytic model. The results herein suggest that the path of this boundary current and the formation of the northern recirculation gyre are sensitive to both the magnitude of lateral viscosity and the strength of the deep western boundary current (DWBC). In particular, it is shown that bottom vortex stretching induced by a downslope DWBC near the south of the Grand Banks leads to the formation of a cyclonic northern recirculation gyre and keeps the path of the depth-integrated western boundary current downstream of Cape Hatteras separated from the North American coast. Both south of the Grand Banks and at the crossover region of the DWBC and Gulf Stream, the downslope DWBC induces strong bottom downwelling over the steep continental slope, and the magnitude of the bottom downwelling is locally stronger than surface Ekman pumping velocity, providing strong positive vorticity through bottom vortex-stretching effects. The bottom vortex-stretching effect is also present in an extensive area in the North Atlantic, and the contribution to the North Atlantic subpolar and subtropical gyres is on the same order as the local surface wind stress curl. Analytic solutions show that the bottom vortex stretching is important near the western boundary only when the continental slope is wider than the Munk frictional layer scale.

1. Introduction

Over the years the problem of the path of the Gulf Stream has inspired many studies, yet a full understanding has remained elusive. Observations show that the Gulf Stream separates from the coast near Cape Hatteras, travels northeast toward the Grand Banks as a free jet in the open ocean, and then part of it turns toward the northeast as the North Atlantic Current. Between Cape Hatteras and the Grand Banks, a barotropic cyclonic northern recirculation gyre (NRG) has been observed just to the north of the Gulf Stream path (Hogg et al. 1986; Fig. 1). The path of the Gulf Stream and the strength of the cyclonic NRG significantly affect the surface heat flux in the western North Atlantic. In addition, warm, salty water transported along the path of Gulf Stream and North Atlantic Current into the subpolar deep-water formation region is very important for the coupled atmosphere–ocean climate system. The north–south shifts of the Gulf Stream path downstream of Cape Hatteras seem related to the North Atlantic Oscillation (NAO) index (Taylor and Stephens 1998; Joyce et al. 2000; Zhang and Vallis 2006). Ezer et al. (1995) found that the Gulf Stream path shifted to the north and the cyclonic NRG was significantly weakened in 1970–74, compared to 1955–59.

As well as being a fundamental problem in oceanography, the separation of the Gulf Stream (often taken as the separation of the depth-integrated North Atlantic western boundary current) has been a vexing issue for modelers; many ocean general circulation models

Corresponding author address: Rong Zhang, NOAA/GFDL, 201 Forrestal Rd., Princeton, NJ 08540.
E-mail: rong.zhang@noaa.gov

DOI: 10.1175/JPO3102.1

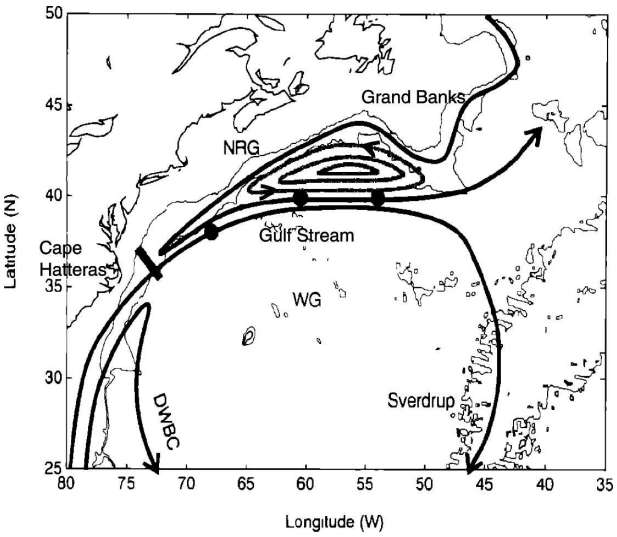

FIG. 1. Schematic diagram of observed barotropic circulation in the western North Atlantic adapted from Hogg (1992).

(OGCMs), including some eddy-permitting models, fail to reproduce the separation and subsequent path of the current properly, and fail to produce the associated cyclonic NRG properly. Frequently, the modeled Gulf Stream stays attached to the U.S. east coast all the way to the Grand Banks, no NRG exists (Dengg et al. 1996), and the modeled North Atlantic Current shifts eastward at the Grand Banks, resulting in a warm bias along the U.S. east coast and a cold bias to the east of Newfoundland; this in turn leads to the need for artificial "flux corrections" in the coupled ocean–atmosphere models (Gerdes et al. 2001).

Motivated, then, by both fundamental and practical issues, our study focuses on the following two questions: 1) what causes the formation of the cyclonic NRG? 2) what keeps the path of the depth-integrated western boundary current downstream of Cape Hatteras separated from the coast? The depth-integrated western boundary current is closely correlated to the near-surface flows at the Gulf Stream region and is often used for diagnoses of the Gulf Stream system properties (Dengg et al. 1996). Early work (Stommel 1948; Munk 1950) predicts that the gyre boundary in the open ocean should be found at the zero line of the Sverdrup transport, and that the western boundary current separates where the Sverdrup transport vanishes at the western boundary. This does not explain the observed separation from Cape Hatteras and the cyclonic NRG just north of the Gulf Stream, because the observed zero line of Sverdrup transport near the western boundary is farther north, close to 50°N. The zero line of Sverdrup transport is also different from the line of zero wind stress curl, because the wind stress curl tilts from southwest to northeast in the North Atlantic (Rhines and Schopp 1991; Böning et al. 1991). Verron and Le Provost (1991) found that the separation of the boundary current is largely independent of the line of zero wind stress curl. Recent studies (Harrison 1989; Ly et al. 1992; Gangopadhyay and Chao 2000) found a strong positive wind stress curl to the north of Gulf Stream. However, even with the high-resolution satellite-observed National Aeronautics and Space Administration (NASA) Quick Scatterometer (QuikSCAT) wind stress (Liu 2002), which has very strong positive wind stress curl to the north of Gulf Stream, the calculated zero line of Sverdrup transport near the western boundary is still farther north than the separation, close to 48°N (shown later in this paper). Evidently surface wind stress curl is not of itself sufficient to produce the separation and subsequent path of the western boundary current at the correct latitude.

Various mechanisms have been suggested for the separation (see Dengg et al. 1996 for a review). Parsons (1969) suggested that the western boundary current separates because of the outcropping of the isopycnal surfaces, and this was supported by the observational study of Gangopadhyay et al. (1992), and further investigated by Jarvis and Veronis (1994). Further studies showed that Parson's separation mechanism must be modified when diabatic heating or cooling are included (Pedlosky 1987; Nurser and Williams, 1990; Chassignet 1995). Rossby (1999) raised the hypothesis that the proper water mass advection from the Labrador region to the Slope Sea is a plausible cause of the southerly excursion of the Gulf Stream path. Hameed and Piontkovski (2004) show that the observed interannual variations of the Gulf Stream north wall lagged the Icelandic low pressure anomaly by 1–3 yr, indicating the impact of Labrador Sea variability on the Gulf Stream shifts. However, the role of the Azores high seems unimportant, perhaps indicating that mechanisms that invoke variations in wind stress in the mid-Atlantic as factors in the variability of the Gulf Stream path are not plausible. Another effect related to Gulf Stream separation is that of inertial overshooting, causing the boundary current to overshoot poleward along the western boundary. This inertial effect has been examined in many idealized numerical models (Bryan 1963; Veronis 1966; Cessi et al. 1990; Dengg 1993; Chassignet 1995; Özgökman et al. 1997), but it has not been conclusively demonstrated that inertial effects can cause Gulf Stream separation at the right latitudes.

Important as the above mechanisms may be, in this

paper our focus is on the importance of bottom topography and the deep western boundary current (DWBC), an effect noted earlier by Mellor et al. (1982) and Greatbatch et al. (1991). They suggested that the interaction between the DWBC and the bottom topography provides positive vorticity via the joint effect of baroclinicity and relief (JEBAR) (Sarkisyan and Ivanov 1971; Holland and Hirschman 1972). Indeed, numerical studies (Thompson and Schmitz 1989; Ezer and Mellor 1992) showed that stronger DWBC results in Gulf Stream separation at lower latitudes. Even with a 1° coarse-resolution model, Gerdes and Köberle (1995) showed that with a strong DWBC obtained by specifying surface density in North Atlantic dense water formation region, the Gulf Stream path downstream of Cape Hatteras can separate from the North American coast. Although the fact that the DWBC affects Gulf Stream separation is well established from the above studies, the physical mechanism is still unclear. For example, Thompson and Schmitz (1989) proposed that at the crossover point of the DWBC and Gulf Stream near Cape Hatteras the DWBC at depth advects the upper Gulf Stream to the south, and Spall (1996) proposed that the entrainment of the upper DWBC has a large influence on the Gulf Stream separation at the crossover. Tansley and Marshall (2000) suggested that the DWBC induces an adverse pressure gradient in the Gulf Stream, and hence its separation at the crossover. However, they also found that it is difficult to distinguish the cause and effect between the separation and the adverse pressure gradient. Sakimoto (2002) suggested that the bottom friction is a key mechanism for producing the bottom downwelling and positive vorticity at the crossover of the DWBC and Gulf Stream. Most of the above-proposed mechanisms focused on the Gulf Stream separation point at the crossover near Cape Hatteras, while the mechanism for the formation of NRG and its role to the Gulf Stream path downstream of Cape Hatteras has not been studied extensively.

In this paper the mechanisms affecting the path of the depth-integrated North Atlantic western boundary current and the formation of NRG are investigated using a hierarchy of models, specifically a prognostic 1° global ocean general circulation model (OGCM) coupled to a two-dimensional atmospheric energy balance model (EBM) with a hydrological cycle, a robust diagnostic model, and a simple barotropic model. We find that the path of the western boundary current and the formation of NRG in our numerical model are quite sensitive both to the magnitude of lateral viscosity and to the strength of the DWBC. In particular, the bottom vortex stretching induced by a downslope DWBC[1] just south of the Grand Banks leads to the formation of a NRG and separates the path of depth-integrated western boundary current downstream of Cape Hatteras from the North American coast. The bottom downwelling induced by the downslope DWBC there is much stronger than the surface Ekman pumping velocity, providing strong positive vorticity through bottom vortex stretching. Our results suggest that the path of the depth-integrated western boundary current downstream of Cape Hatteras is greatly affected by the strength of the NRG, and thus the DWBC near the south of the Grand Banks, not specifically by the processes at the precise crossover region near Cape Hatteras. This is consistent with the observations that there is little change in the separation point at Cape Hatteras on decadal time scales, while major decadal variations are found in the north–south shifts of the separated path downstream of Cape Hatteras (Joyce et al. 2000). Strong bottom downwelling induced by the downslope DWBC also appears at the crossover of the DWBC and Gulf Stream near Cape Hatteras in our numerical experiments when the DWBC there is relatively strong. An analytical model and a simple numerical barotropic model suggest that bottom vortex stretching at the crossover contributes to the separation of the depth-integrated western boundary current at Cape Hatteras. The analytical model shows that with a continental slope that is wider than the Munk layer scale, the bottom vortex stretching, which is related to the bottom pressure torque, dominates the western boundary [consistent with Hughes and De Cuevas (2001), who show that that the bottom pressure torques dominate the western boundary and balance surface wind stress curl when the continental slope width is larger than the Munk layer scale].

The paper is organized as follows. In section 2, we discuss the diagnostic modeling results of North Atlantic Ocean circulation. In section 3, we describe the prognostic modeling results and compare them with the diagnostic modeling results. In section 4, we propose a theoretical mechanism of the formation of NRG and the path of the depth-integrated western boundary current downstream of Cape Hatteras, and the role of bottom vortex stretching in the vicinity of the western boundary. We compare the modeling results with the proposed mechanism in section 5, and test the theory

[1] Throughout this paper, the expression "downslope current" refers to a horizontal current projected on the downslope direction, which is a direction perpendicular to the isobaths on the horizontal plane

with a simple barotropic model (in section 6) and with an analytical model (in section 7).

2. North Atlantic circulation from a diagnostic calculation

To obtain an approximation of a realistic ocean circulation in the North Atlantic, a "robust diagnostic" calculation is first carried out, in which the global model potential temperature and salinity are strongly relaxed back to the observed annual mean climatology (Levitus et al. 2000). The method may be regarded as a way of assimilating the observed hydrographic fields and producing dynamically consistent three-dimensional velocity and pressure fields. To do this we employed a global OGCM coupled to a two-dimensional atmospheric EBM with a simple hydrological cycle and to a slab sea ice model (Winton 2000). The details are described in appendix A. The restoring of model potential temperature and salinity is very strong, with a time scale of ~1 day. The lateral viscosity and background vertical viscosity we used are $A_H = 1.42 \times 10^4\ \mathrm{m^2\,s^{-1}}$ and $A_V = 1 \times 10^{-4}\ \mathrm{m^2\,s^{-1}}$, respectively. The model is driven by the Comprehensive Ocean–Atmosphere Dataset (COADS) climatological annual mean surface wind analyzed by Da Silva et al. (1994).

The diagnostic model reached equilibrium on a time scale of about a month. Figure 2 shows the current at 75 m and the barotropic streamfunction at the end of the 60-day run. In this calculation the depth-integrated western boundary current separates from the coast near Cape Hatteras, similar to what is observed, although the cyclonic NRG has a strength of ~6 Sv (1 Sv $\equiv 10^6\ \mathrm{m^3\,s^{-1}}$), which is much smaller than the observations and previous diagnostic calculations (~20 Sv) that use vertically averaged equations of motion (Mellor et al. 1982; Greatbatch et al. 1991). The North Atlantic Current moves northeastward near the Grand Banks. The maximum depth-integrated transport across the Gulf Stream is about 44 Sv, which is much larger than that predicted by the Sverdrup theory, although it is still much smaller than the observations and previous diagnostic calculations (~90 Sv) (Mellor et al. 1982; Greatbatch et al. 1991). The smoothed topography and climatological temperature/salinity used in the model may be part of the cause thereof. The lateral viscous term employed in this coarse-resolution model also reduces the strength of the transport of the depth-integrated western boundary current. The robust diagnostic model also produces the anticyclonic southern recirculation gyre, that is, the Worthington gyre (WG) (Worthington 1976), at the observed location (near 35°N, 55°W), which is often missing in prognostic OGCMs.

3. North Atlantic Ocean circulation from a prognostic model

It is well known that it is very difficult for prognostic OGCMs to properly simulate the separation and subsequent path of the Gulf Stream. It is not unusual for a modeled Gulf Stream to stay attached to the U.S. east coast all the way to the Grand Banks (Dengg et al. 1996), and the modeled North Atlantic Current then moves more directly eastward, resulting in a warm bias along the U.S. east coast and a cold bias at the east of Newfoundland, and, consequently, unrealistic air–sea heat and freshwater fluxes. Increasing the resolution and permitting the formation of eddies does not, in itself, necessarily help. For example, Smith et al. (2000) found that the modeled Gulf Stream did not separate properly even with 0.28° horizontal resolution, and a strong anticyclonic eddy forms at northeast of Cape Hatteras, which seems to be a common feature of many marginally eddy-permitting simulations (Dengg et al. 1996). The modeled Gulf Stream did separate at the right place with some 0.1° horizontal resolution models (Smith et al. 2000), which might seem to imply that fully eddy-resolving models may be necessary to get proper separation, but we shall offer an alternative explanation.

a. Model description

We employ the same simple global coupled model as that used in the diagnostic calculations (appendix A) to conduct some prognostic experiments, that is, with no restoration of the ocean potential temperature and salinity. In particular, the OGCM has the same global configuration, realistic bathymetry, and horizontal/vertical resolution as that in the robust diagnostic calculation. The coupled model was spun up from an initial condition of rest with zonally averaged Levitus temperature and constant salinity in the ocean and a climatological sea ice distribution, with a specified wind stress and wind speed. The EBM provides the thermodynamic forcing. All experiments were spun up asynchronously (i.e., using a different time step for ocean tracer and momentum) for 35 yr, followed by a synchronous spinup for another 10 yr to avoid any distortion of the seasonal cycle with asynchronous time stepping (Danabasoglu et al. 1996). After the 45-yr spinup, the thermohaline circulation is stabilized, and the results we show in the following subsection are the annual mean of the last year of the total 45-yr spinup.

b. Model results

Figure 3 shows the current at 75 m (below the Ekman layer) and the barotropic streamfunction in the North

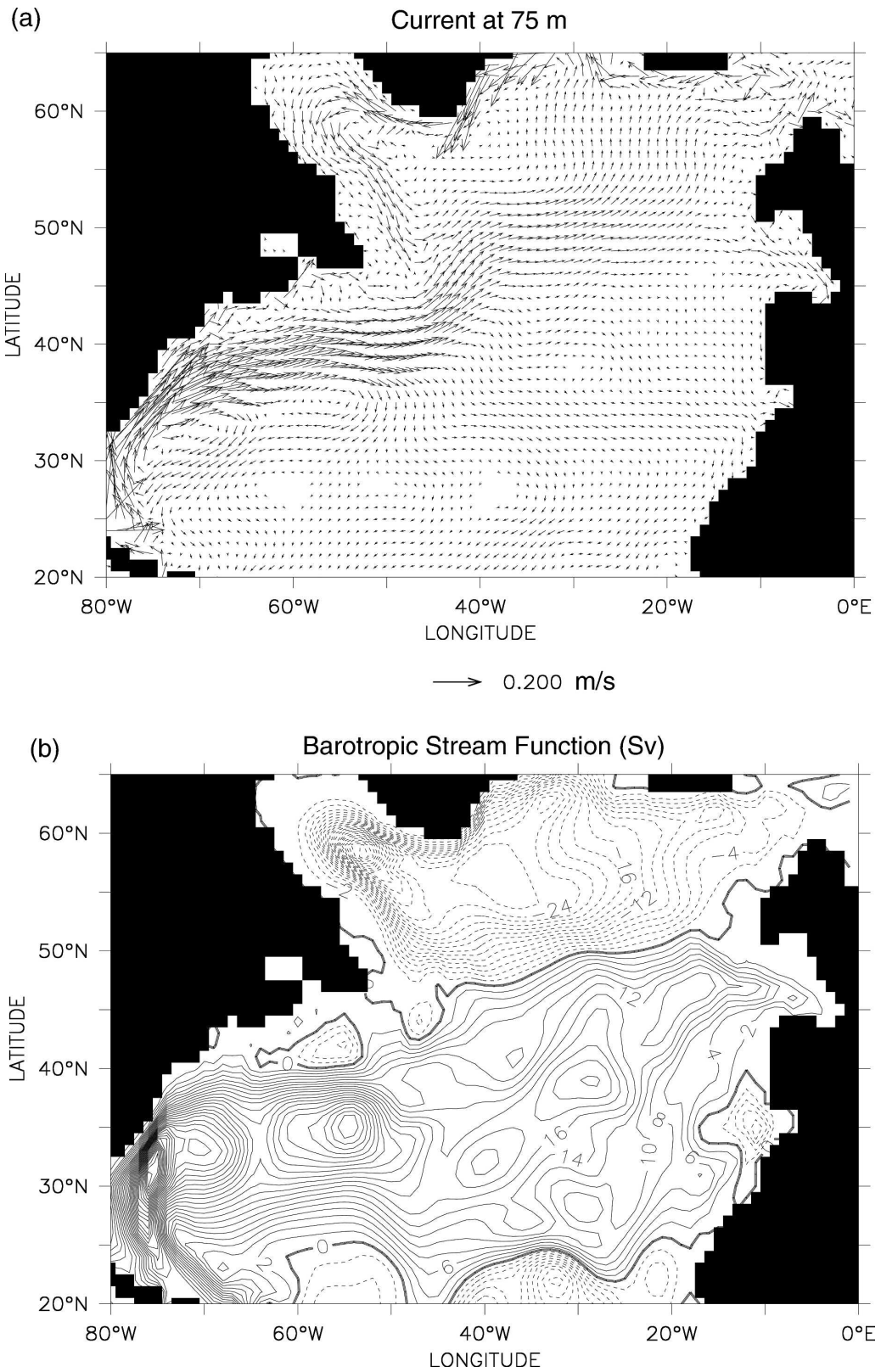

FIG. 2. North Atlantic circulation in the robust diagnostic calculation: (a) current at 75 m and (b) barotropic streamfunction (Sv; contour interval is 2 Sv).

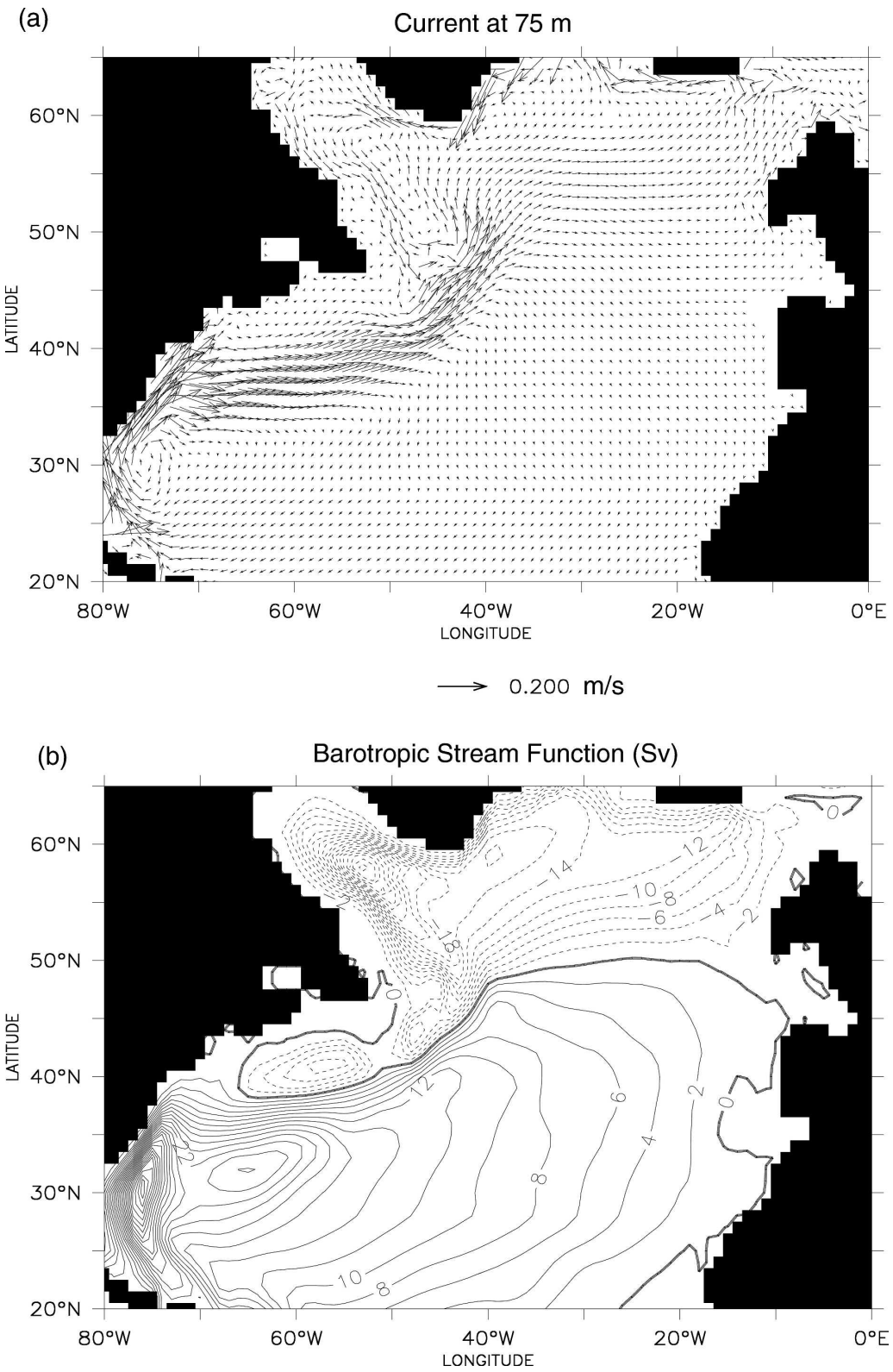

FIG. 3. North Atlantic circulation in experiment I, control run: (a) current at 75 m and (b) barotropic streamfunction (Sv; contour interval is 2 Sv).

TABLE 1. Main physical parameters and forcing of prognostic experiments.

Parameters and forcing	Expt I	Expt II	Expt III	Expt IV	Expt V
Lateral viscosity A_H ($m^2 s^{-1}$)	1.42×10^4	1.42×10^5	1.42×10^4	1.42×10^4	1.42×10^4
Atmospheric solar radiation absorption coefficient a_{abs}	0.25	0.25	0.32	0.25	0.25
Surface wind stress	COADS	COADS	COADS	ECMWF AMIP	ECMWF AMIP
Surface wind speed	COADS	COADS	COADS	ECMWF AMIP	COADS

Atlantic of the control run (experiment I; see Table 1 for a list of parameters). In this control run, the model is forced with COADS climatological monthly mean surface wind stress and wind speed. North of Cape Hatteras the path of the depth-integrated western boundary current remains separated from the North American coast, and there is a cyclonic NRG (~9 Sv) to the north. These results are very similar to the robust diagnostic calculation (Fig. 2). The Gulf Stream overshoots a little to the north near Cape Hatteras, as found in many previous modeling studies. However, the slight overshooting near Cape Hatteras does not lead to the northward shift of the Gulf Stream path downstream of Cape Hatteras; in fact, the path downstream of Cape Hatteras is a little farther south than the observations suggest, indicating that the Gulf Stream path downstream of Cape Hatteras is not dominated by processes occurring at the crossover region near Cape Hatteras. After passing the Grand Banks, part of the Gulf Stream turns northward becoming the North Atlantic current (Fig. 3a), transporting warm, salty water to the east of Newfoundland. In this experiment, the maximum thermohaline circulation is not especially strong, about 16 Sv. However, the modeled DWBC *is* relatively strong and the lateral viscosity is as small as possible for the given horizontal resolution to avoid numerical noise ($A_H = 1.42 \times 10^4$ $m^2 s^{-1}$). Hence, with a sufficiently strong and narrow DWBC it is evidently possible for a non-eddy-resolving model to obtain a separated path of the depth-integrated western boundary current downstream of Cape Hatteras and the cyclonic NRG.

1) SENSITIVITY TO LATERAL VISCOSITY

To test the sensitivity of Gulf Stream system properties to the magnitude of lateral viscosity, we repeated the experiment with much higher viscosity (experiment II), $A_H = 1.42 \times 10^5$ $m^2 s^{-1}$, a value that is typically used in $2° \times 2°$ OGCMs. The model is again forced with COADS climatological monthly mean surface wind stress and wind speed. In this case, both the Gulf Stream and the DWBC are too weak and too wide. The Gulf Stream stays attached to the coast, no NRG exists, and the subtropical–subpolar gyre boundary is near the zero line of the Sverdrup transport (Fig. 4). The North Atlantic Current moves more zonally, resulting in colder sea surface temperatures (SSTs) to the east of Newfoundland.

2) SENSITIVITY TO THE STRENGTH OF THE DWBC

We tested the sensitivity of the Gulf Stream system properties to the strength of the DWBC in experiment III, in which the strength of the thermohaline circulation and the DWBC are modulated by the atmospheric solar radiation absorption coefficient a_{abs} in the EBM (appendix A); the polar surface air temperature is very sensitive to a_{abs}. With larger a_{abs}, more solar radiation is absorbed in the atmosphere, and the polar surface air temperature is warmer, reducing the buoyancy flux there and resulting in a reduction of the deep-water formation rate. In this experiment, a_{abs} is increased from 0.25 to 0.32 (Table 1), the maximum thermohaline circulation is reduced to 11Sv, and the DWBC is correspondingly weakened. The consequence of this is the vanishing of the cyclonic NRG and that the poleward shifts of the path of the Gulf Stream (Fig. 5). Evidently, the path of the Gulf Stream and the strength of NRG are very sensitive to the DWBC strength.

3) SENSITIVITY TO SURFACE WIND FORCING

A recent modeling study by Gangopadhyay and Chao (2000) suggested that a strong positive wind stress curl at the north of the Gulf Stream may be very important for the Gulf Stream separation. We tested the sensitivity to surface wind with the same model setup as that in our control run (experiment I), except that the model is forced with the 1979–95 climatological surface wind from the Atmospheric Model Intercomparison Project (AMIP) II integration (Gates 1992) and with the European Centre for Medium-Range Weather Forecasts (ECMWF) operational model (ECMWF 1991); this constitutes experiment IV (Table 1). This surface wind product has stronger wind stress curl in both the subpolar and subtropical gyres compared to that of the COADS wind (appendix C), but the wind

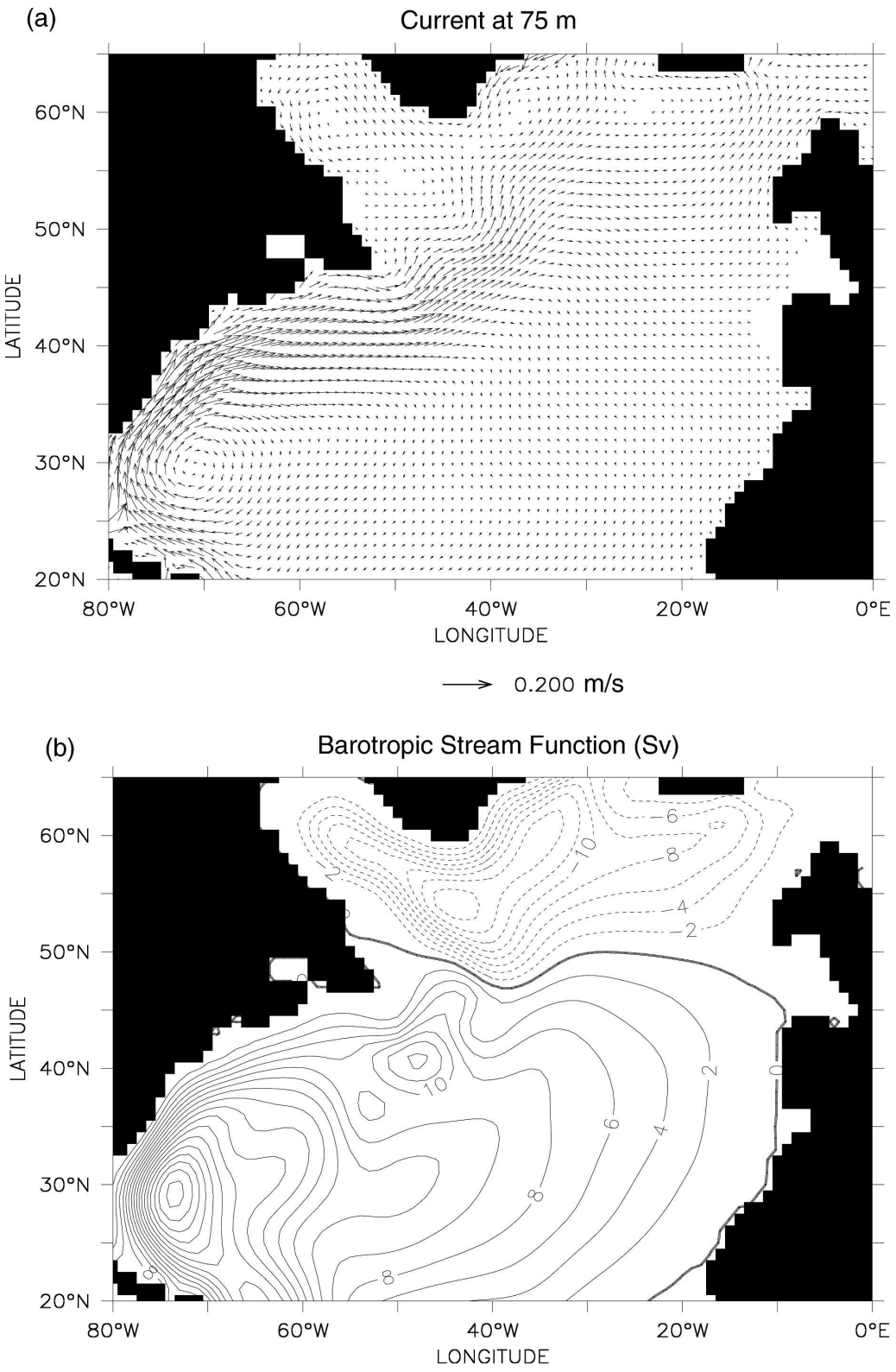

FIG. 4. North Atlantic circulation in experiment II, higher lateral viscosity: (a) current at 75 m and (b) barotropic streamfunction (Sv; contour interval is 2 Sv).

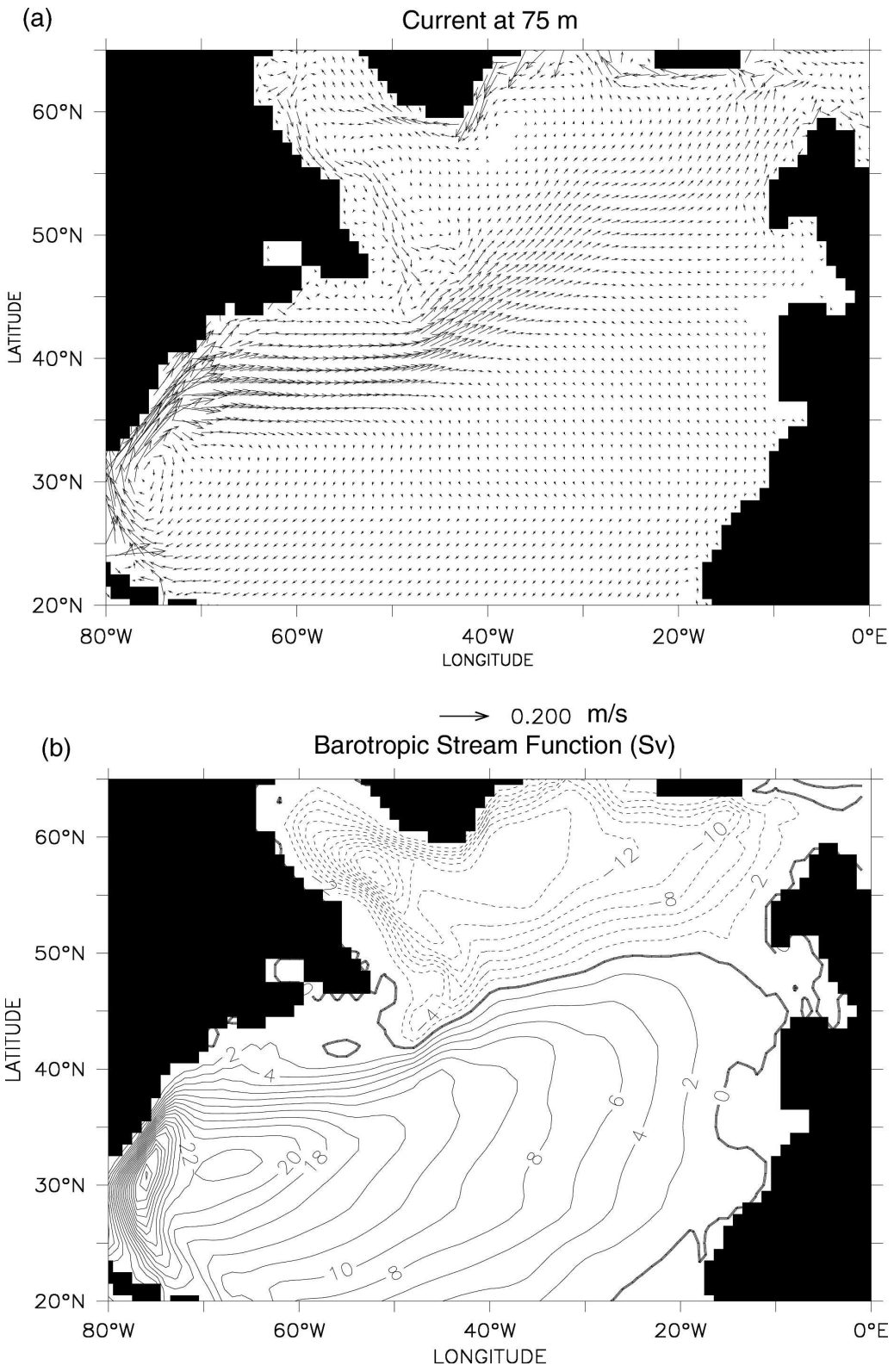

FIG. 5. North Atlantic circulation in experiment III, weaker DWBC: (a) current at 75 m and (b) barotropic streamfunction (Sv; contour interval is 2 Sv).

speed is much weaker, because it is derived from the monthly mean surface wind vector. In the coupled model surface wind *speeds* are used in the bulk formulas to compute ocean surface sensible heat flux and evaporation, so that weaker surface wind speed will significantly reduce the surface buoyancy flux in the Labrador Sea and weaken the deep convection, and thus, potentially, weaken the DWBC. Hence, the experiment explores the relative importance of the wind speed versus the wind stress curl.

The model results show that the Gulf Stream stays attached to the coast and no NRG is produced (Fig. 6), although the subpolar gyre is stronger and the subtropical–subpolar gyre boundary in the open ocean is shifted southward (to 45°N) because of the stronger positive wind stress curl in the subpolar region. Hence, the strong positive subpolar wind stress curl is not of itself sufficient to produce the separation and subsequent path of the Gulf Stream at the correct latitude. The deep convection in Labrador Sea in this experiment is much weaker than that observed and that in experiment I. The mixed layer depth in center Labrador Sea is only about 500 m now; much shallower than that in experiment I (where it was more than 2000 m). The DWBC in this experiment is also much weaker compared to that in experiment I. It is reasonable to conclude that the lack of the NRG and the northward shift of the path of the depth-integrated western boundary current with ECMWF AMIP II winds is due to differences in wind speed over the Labrador Sea that give rise to too weak a convection and too weak a DWBC.

To test this hypothesis more thoroughly, we conducted one further experiment (experiment V), in which the model is forced with the same ECMWF AMIP II surface wind stress, but with COADS surface wind speed, and all other forcings and parameters are the same as in experiment I. (As noted above, the wind speed affects the surface fluxes via the bulk aerodynamic formulas.) The solution is found to be very similar to experiment I; that is, the path of the depth-integrated western boundary current downstream of Cape Hatteras separates from the North American coast, and the cyclonic NRG appears again with a strength of about 11Sv (Fig. 7). The deep convection in Labrador Sea is quite strong now, with a mixed layer depth of more than 2000 m; the DWBC is also quite strong, resulting from the strong COADS wind speed, leading to the cyclonic NRG and separated path of the depth-integrated western boundary current downstream of Cape Hatteras, and resembles that of experiment I more than that of experiment IV. The result indicates that the influence of the wind speed on convection in the subpolar gyre, and consequently on the strength of the DWBC, is relatively more important than the wind stress in keeping the path of the depth-integrated western boundary current downstream of Cape Hatteras separated from the coast.

4) SUMMARY OF PROGNOSTIC MODELING RESULTS

The prognostic experiments show that the ocean circulation in the North Atlantic is very sensitive to both the magnitude of lateral viscosity and the strength of the DWBC. Both experiments I and V, which have relatively low lateral viscosity and strong DWBC, were able to obtain a separated path of the depth-integrated western boundary current downstream of Cape Hatteras and the cyclonic NRG similar to that of the robust diagnostic calculation. Figure 8 shows the Gulf Stream across the vertical section (60°W) in all prognostic experiments and the robust diagnostic calculation. The Gulf Stream in the robust diagnostic calculations, experiments I and V (Figs. 8a,b,f) are much stronger and deeper than those in experiments II, III, and IV (Figs. 8c,d,e). In experiments I and V (Figs. 8b,f), the Gulf Stream axis is separated from the coast, similar to that in the robust diagnostic calculation (Fig. 8a); while in experiments II, III, and IV (Figs. 8c,d,e) the Gulf Stream axis is attached to the coast. The stronger, narrower westward flow in the deeper ocean, that is, the DWBC, appears off the continental slope north of the Gulf Stream in the robust diagnostic calculations of experiments I and V (Figs. 8a,b,f), while in experiments II, III, and IV (Figs. 8c,d,e) the DWBC is much weaker.

Note that both experiments IV and V are forced with the same ECMWF AMIP II surface wind stress, and the only difference between the two experiments is the surface wind speed, which leads to different deep convection in the Labrador Sea, different DWBCs, and different NRGs and Gulf Stream paths; both experiments I and V are forced with the same COADS surface wind speed, which leads to very similar deep convection in Labrador Sea and DWBCs, and very similar NRGs and Gulf Stream paths, although the two experiments are forced with different surface wind stress. This indicates that the direct dominant factor affecting the formation of the NRG and the separated Gulf Stream path downstream of Cape Hatteras is the strength of the DWBC, not the surface wind stress curl.

Finally, we note that the EBM is not important in itself other than being a convenient way to obtain reasonably realistic forcing—coupling to the EBM provides a much better way to simulate the surface buoyancy flux than typical techniques used in ocean-only

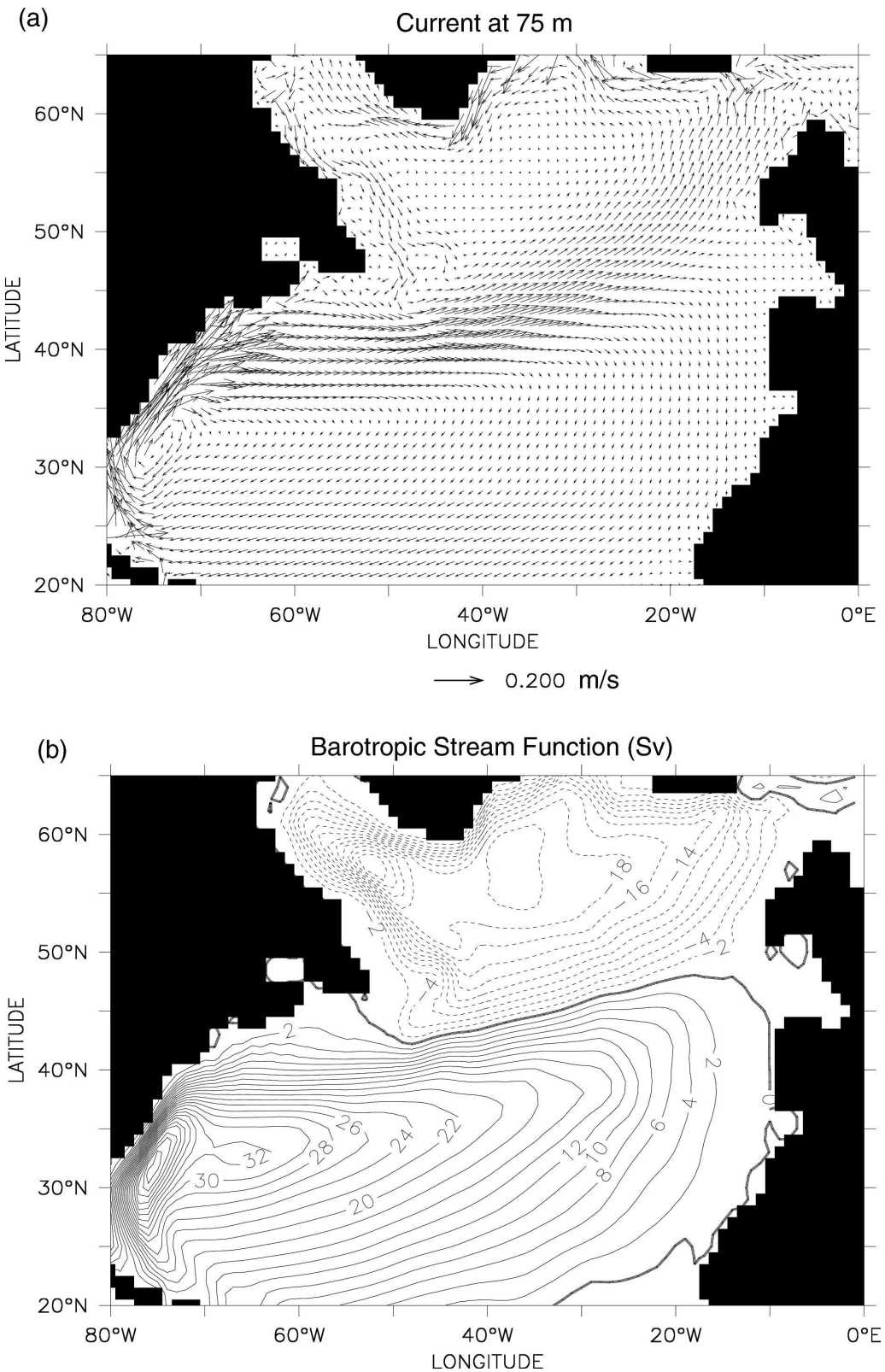

FIG. 6. North Atlantic circulation in experiment IV, ECMWF AMIP II wind stress and weak wind speed: (a) current at 75 m and (b) barotropic streamfunction (Sv; contour interval is 2 Sv).

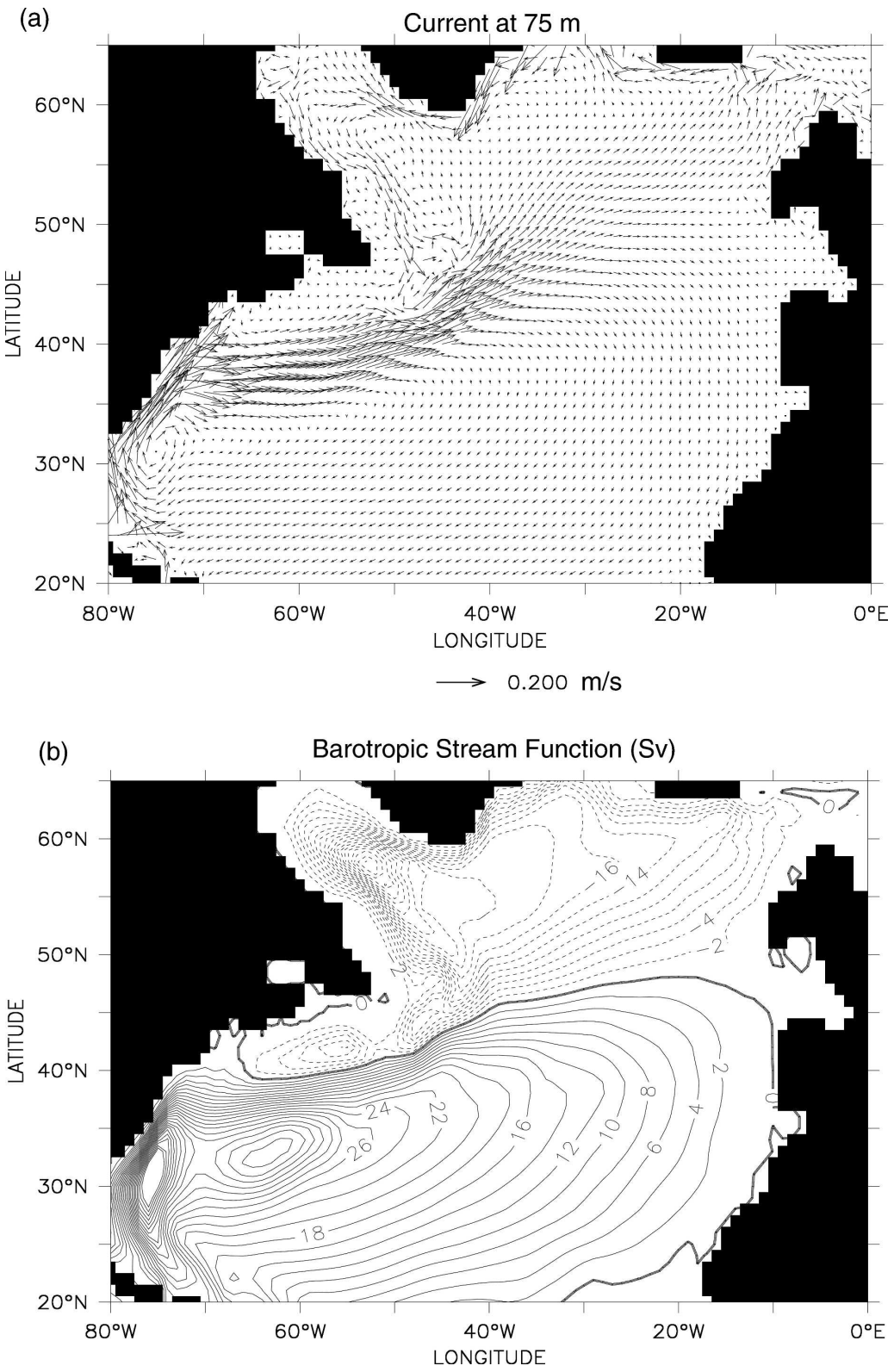

FIG. 7. North Atlantic circulation in experiment V, ECMWF AMIP II wind stress and COADS wind speed: (a) current at 75 m and (b) barotropic streamfunction (Sv; contour interval is 2 Sv).

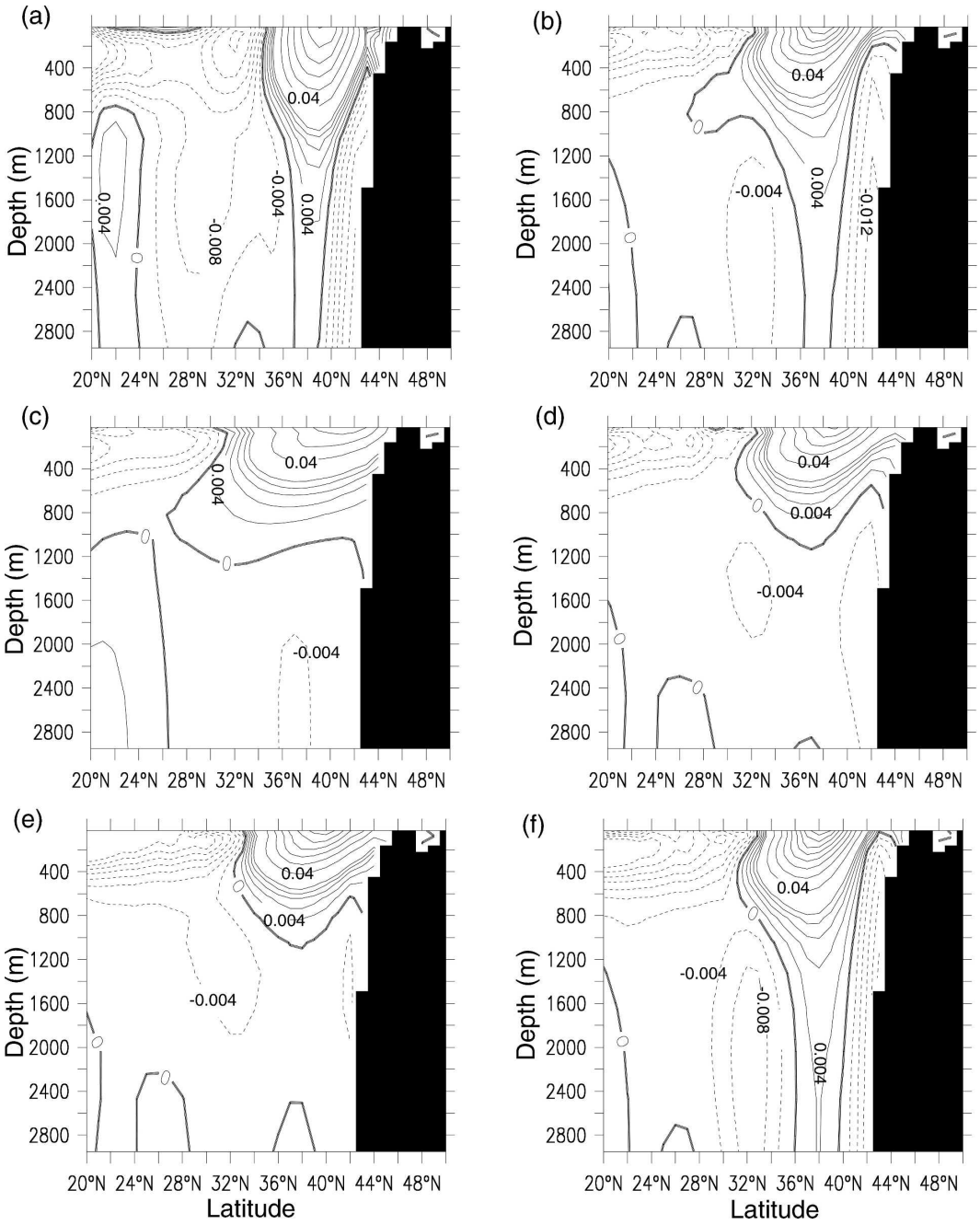

FIG. 8. Zonal flow at the vertical section of 60°W (contour interval is 0.004 m s^{-1} when $u \leq 0.02$ m s^{-1} and 0.02 m s^{-1} when $u > 0.02$ m s^{-1}). (a) Robust diagnostic calculation; (b) experiment I, control run; (c) experiment II, higher lateral viscosity; (d) experiment III, weaker DWBC; (e) experiment IV, ECMWF AMIP II wind stress and weak wind speed; and (f) experiment V, ECMWF AMIP II wind stress and COADS wind speed.

models. For example, if instead of coupling the OGCM to the EBM, the surface temperature and salinity are restored to observed climatology (Levitus et al. 2000), then the surface buoyancy flux is only affected by the restoring terms. This gives an unrealistically weak surface buoyancy flux and thus unrealistically weak deep convection in the Labrador Sea. The result of this is that the modeled maximum thermohaline circulation is very weak, only about 4 Sv; the modeled DWBC is concomitantly weak, and there is no NRG and the Gulf Stream is attached to the coast from Cape Hatteras all the way to Newfoundland.

4. A simple mechanism for the NRG and path of the western boundary current

We now consider a simple mechanism that affects the NRG and path of the depth-integrated western boundary current. Our model is illustrative, rather than wholly quantitative, and we begin with the vertical integration of the steady linear vorticity equation of a homogeneous ocean with the β plane approximation, that is,

$$\beta \frac{\partial \Psi}{\partial x} = \frac{\mathbf{k} \cdot \nabla \times \boldsymbol{\tau}}{\rho_0} + A_H \nabla^4 \Psi - f_0 W_B, \qquad (4.1)$$

where Ψ is the streamfunction of the vertically integrated flow (the "barotropic streamfunction") such that

$$\frac{\partial \Psi}{\partial x} = \int_{-H}^{0} v \, dz \quad \text{and} \quad \frac{\partial \Psi}{\partial y} = -\int_{-H}^{0} u \, dz. \qquad (4.2)$$

Here H is water depth (which varies sharply near the Gulf Stream region), $\nabla \times \boldsymbol{\tau}$ is the surface wind stress curl, A_H is the lateral viscosity that we assume vanishes at the ocean bottom, ρ_0 is the mean ocean density, f_0 is the constant Coriolis parameter, and W_B is the bottom vertical velocity induced by Ekman friction and bottom flow $\mathbf{u}_B$ across topographic isobath, that is,

$$W_B = \frac{\delta_E}{2} \zeta_B - \mathbf{u}_B \cdot \nabla H, \qquad (4.3)$$

where ζ_B is the bottom relative vorticity and δ_E is the bottom Ekman layer thickness.

We use a vertically integrated model because our diagnoses are focused on the vertically integrated transport over the whole ocean column. Such transport (i.e., the barotropic streamfunction) is closely correlated to the near-surface flows in the Gulf Stream region, and many previous simulations of Gulf Stream separation have been judged by it (Dengg et al. 1996). When the bottom vertical velocity is large enough, the ocean's vertically integrated transport in the basin interior will differ from the Sverdrup transport; that is, the transport will depend not only on the surface boundary condition (wind stress curl), but also on the vertical velocity at the bottom (W_B). We thus need both surface and bottom boundary conditions to get the vertically integrated transport through the whole ocean column, even though the real ocean is baroclinic and much of that barotropic transport may be manifest in the upper ocean.

The importance of the bottom boundary condition in influencing the path of the Gulf Stream has been suggested previously. For example, Sakimoto (2002) suggested that the bottom downwelling induced by Ekman friction ($\delta_E \zeta_B/2$) at the crossover of the DWBC and the Gulf Stream produces the positive vorticity and contributes to Gulf Stream separation, but he did not consider the role of continental slope in producing bottom downwelling. In fact, the topographically induced vertical velocity, $-\mathbf{u}_B \cdot \nabla H$, is likely to dominate the frictionally induced one in region from Cape Hatteras to the Grand Banks over steep continental slopes, essentially because, provided that the flow goes across the topography, the ratio of the two is equal to the ratio of variations in topographic height to the Ekman layer thickness (Vallis 2006). The Ekman layer thickness depends on the magnitude of the vertical turbulent viscosity but is unlikely to exceed 100 m, and is likely much less, whereas topographic heights vary by the order of 1km.

Observations indicate that the DWBC does indeed cross the topography; Bower and Hunt (2000) analyzed the trajectories of RAFOS floats launched in the DWBC between the Grand Banks and Cape Hatteras and found that the DWBC in the crossover region moves downslope with a (horizontal) speed on the order of 5 cm s^{-1}. Consistently, directly observed DWBC velocities in the Gulf Stream region from current meter measurements are in the range from 5 to ~10 cm s^{-1} (Hogg et al. 1986; Pickart and Watts 1990), and using hydrographic data Pickart and Smethie (1993) found that most of the upper Labrador Seawater transported by the DWBC was significantly diverted downslope at the crossover region. Horizontal speeds (U) of this magnitude give rise to bottom vertical velocities of the order of $W_B \sim UH/L \approx 10^{-4}$ m s^{-1}, where H/L is the continental slope near Cape Hatteras. In our robust diagnostic calculation, the averaged bottom downwelling at the crossover region of the Gulf Stream and the DWBC (Fig. 9a) is on the order of 3×10^{-5} m s^{-1}. The continental slope at the crossover region is on the order of 10^{-2}, and the simulated downslope DWBC speed there is on the order of 4×10^{-3} m s^{-1}; thus, the scaling estimate of bottom downwelling (4×10^{-5} m s^{-1}) is consistent with the actual value. The vertical velocity induced by a wind stress curl is, on the other hand, typically about 10^{-6} m s^{-1}. All of this suggests that the magnitude of bottom downwelling induced by the downslope DWBC may well be larger than the surface Ekman pumping velocity.

With the geostrophic approximation, we have

$$W_B \approx -\mathbf{u}_B \cdot \nabla H \approx -J(\psi_B, H) = -\frac{J(P_B, H)}{f_0 \rho_0}. \qquad (4.4)$$

Thus, the bottom vortex-stretching term $-f_0 W_B$ is directly linked to the bottom pressure torque $J(P_B, H)$.

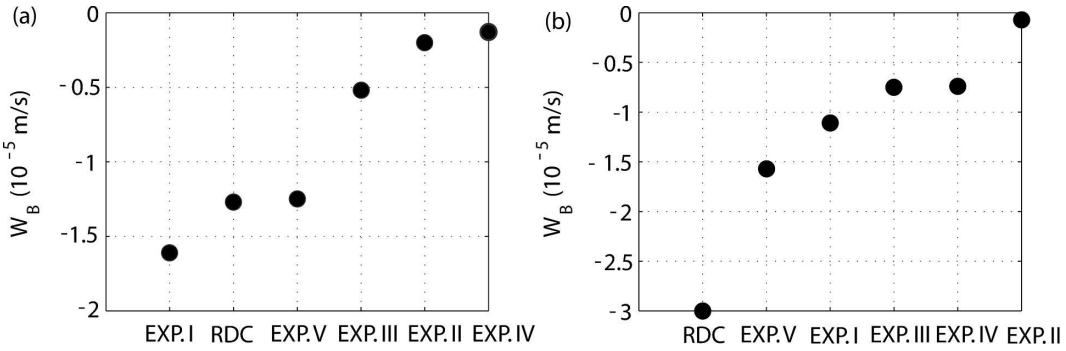

FIG. 9. Plot of averaged bottom vertical velocity W_B (10^{-5} m s^{-1}) from all experiments. (a) Around the western boundary near Grand Banks (44°–45°N, 47°–46°W). (b) Around the crossover of Gulf Stream and DWBC near Cape Hatteras (36°N, 73°–72°W). RDC: robust diagnostic calculation; experiments I–V same as in Fig. 8.

Here P_B is the bottom pressure and $\psi_B = P_B/(f_0\rho_0)$ is the bottom streamfunction. Although W_B is dominated by the downslope DWBC near steep topography, the bottom friction is important in making DWBC actually move downslope; otherwise, the flow will follow f/H contours. When the DWBC meets the Gulf Stream near Cape Hatteras, a strong anticyclonic shear is formed; the bottom friction induces a divergence and thus downslope DWBC. Over the steep continental slope there, the downslope DWBC leads to strong bottom downwelling and thus a positive vorticity through bottom vortex stretching, contributing to the separation of the depth-integrated western boundary current from the coast. When the DWBC passes through the south of the Grand Banks, the sharp curvature of isobaths and steep topographic slope there induce anticyclonic flow; the bottom friction there again induces a divergence and thus a downslope DWBC. The bottom vertical velocity directly induced by the bottom friction ($W_B = \delta_E\zeta_B/2$) is much smaller than the bottom vertical velocity induced by the downslope DWBC near the steep continental slope ($W_B = -\mathbf{u}_B \cdot \nabla H$). If the ocean bottom were nearly flat, then W_B would be dominated by the term ($\delta_E\zeta_B/2$) induced directly by the bottom friction. The downslope DWBC south of the Grand Banks leads to strong bottom downwelling resulting from the steep continental slope there and thus a positive vorticity through bottom vortex stretching; this contributes to the formation of the NRG, which keeps the path of the depth-integrated western boundary current downstream of Cape Hatteras separated from the North American coast.

5. Comparison with modeling results

We now compare our modeling results with the mechanism of the previous section. The strong bottom downwelling near Cape Hatteras and the Grand Banks are found not only in our robust diagnostic calculation, but also in the prognostic modeling results that have strong DWBC, that is, experiments I and V (Fig. 9), and the bottom downwelling there is of the same order or even larger than the surface Ekman pumping velocity. In experiment II, with high viscosity and thus weaker and broader DWBC, no significant bottom downwelling is excited near the topographic slope (Fig. 9). In experiments III and IV with weaker DWBC, the bottom downwelling near the topographic slope is also weaker than that in experiments I and V (Fig. 9).

The strength of the DWBC across the zonal section at the south of the Grand Banks and at Cape Hatteras from all experiments is compared in Fig. 10. The deep current along the western boundary (48°W) near the south of the Grand banks is stronger both in experiments I and V and the robust diagnostic calculation, and is much weaker in experiments II, III, and IV (Fig. 10a). This is consistent with the bottom downwelling (Fig. 9) at the western boundary near the Grand Banks being stronger both in experiments I and V and the robust diagnostic calculation than in experiments II, III, and IV. The stronger bottom downwelling contributes to the formation of the cyclonic NRG and the southward shift of the path of the depth-integrated western boundary current downstream of Cape Hatteras in experiments I and V and to the robust diagnostic calculation. The deep current along the western boundary (73°W) near Cape Hatteras is stronger in experiments I and V, and much stronger in the robust diagnostic calculation, compared to experiments II, III, and IV (Fig. 10b). This is consistent with the results that bottom downwelling (Fig. 9) near Cape Hatteras is stronger in experiments I and V and much stronger in the robust diagnostic calculation, relative to that in experiments II, III, and IV.

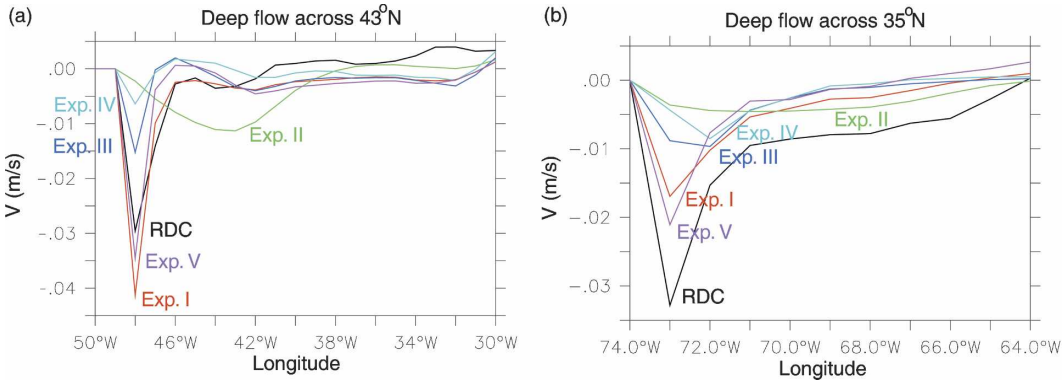

FIG. 10. Deep flow (meridional velocity at the depth of 2470 m, m s^{-1}) across a zonal section across (a) 43° and (b) 35°N. RDC: robust diagnostic calculation; experiments I–V same as in Fig. 8.

Figure 11(a) shows that the DWBC is stronger in experiment I all the way from the deep Labrador Sea to the region south of the Grand Banks, and the anticyclonic shear induced by the northward Gulf Stream penetrating to this deep level and the southward DWBC near Cape Hatteras is also stronger than that in experiment III. In a vertical section across 43°N near the Grand Banks (Fig. 11b), the meridional southward flow in experiment I is stronger in the deeper ocean near the western boundary, with the core of this enhanced DWBC located below 2000 m, and the increasing northward flow at the upper ocean centered around 46°W shows that the northward North Atlantic Current (NAC) offshore is also stronger in experiment I. This is consistent with observations that the stronger southward DWBC near the Grand Banks is associated with stronger northward NAC offshore (Schott et al. 2004). A recent 0.1° eddy-resolving model simulation with the Los Alamos National Laboratory Parallel Ocean Program (POP) shows a similar relationship between the southward DWBC and northward offshore NAC near the Grand Banks (M. Hecht 2004, personal communication).

The middomain bottom flow in experiment I (near 32°N, 60°W; Fig. 11a) is unrealistic in this 1° model in that part of the modeled deep flow moves south in the interior ocean instead of moving along the western boundary, and thus this interior large-scale flow actually weakens the DWBC near Cape Hatteras in this 1° prognostic model. That is why the DWBC near Cape Hatteras is much stronger in the robust diagnostic calculation than in the prognostic modeling results of experiments I and V (Fig. 10b). Hence, the averaged bottom downwelling, and thus vortex stretching, near Cape Hatteras (Fig. 9) is 3×10^{-5} m s^{-1} in the robust diagnostic calculation, which is much stronger than that in experiments I and V. The stronger bottom downwelling near Cape Hatteras contributes to the separation of the depth-integrated western boundary current at Cape Hatteras as shown later with a simple numerical barotropic model (section 6) and an analytical model (section 7).

The above numerical results are largely consistent with the theory that the strong bottom downwelling induced by the downslope DWBC near topography south of the Grand Banks aids in the formation of NRG and the separated path of the depth-integrated western boundary current downstream of Cape Hatteras.

6. Testing the theory with a barotropic model

To explore the validity of the simple theory, we employed a simple barotropic model [modified from the fourth Modular Ocean Model (MOM4)] to numerically solve the vertically integrated vorticity equation, namely,

$$\beta \frac{\partial \Psi}{\partial x} = \frac{\mathbf{k} \cdot \nabla \times \boldsymbol{\tau}}{\rho_0} + A_H \nabla^4 \Psi - f_0 W_B. \qquad (6.1)$$

The barotropic model has constant density and a flat bottom with a uniform depth of 400 m. The model has the geometry of North Atlantic (from 20° to −65°N, from 80°W to −0°), with 1° × 1° resolution in the horizontal and a solid wall boundary with no-slip condition. The model is forced with an observed annual mean surface wind. Because the model is barotropic, the bottom vortex-stretching term, that is, the term $f_0 W_B$, is diagnosed from the full three-dimensional OGCMs and can be added into the model directly as a vertical component of stress curl, just like that of surface wind stress curl. The lateral viscosity is the same as that in the diagnostic calculation. Before proceeding, let us make two comments about the model: first, in (6.1), no JEBAR term arises explicitly; second, we are interested

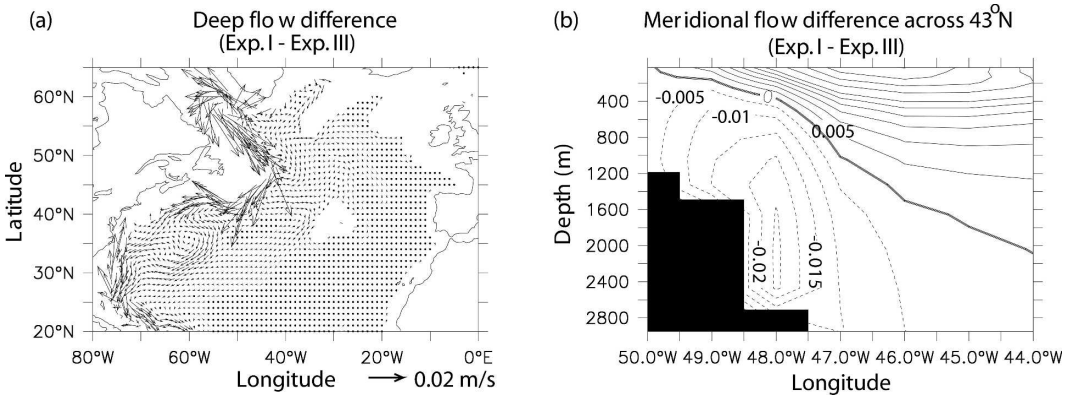

FIG. 11. Current differences between experiments I and III (experiment I − experiment III): (a) deep current difference at the depth of 2470 m, and (b) meridional flow difference across the zonal section of 43°N (contour interval is 0.005 m s^{-1} when $v \leq 0.03$ m s^{-1}; contour interval is 0.01 m s^{-1} when $v > 0.03$ m s^{-1}). The dashed contours at lower left correspond to the DWBC, and the solid contours at upper right correspond to the North Atlantic Current.

in the vertically integrated transport, for which the bottom velocity is the relevant one.

Figure 12 shows the equilibrium barotropic streamfunction for the cases with COADS surface wind stress. With only surface wind stress and $W_B = 0$ (Fig. 12a), the solution is just the Munk boundary layer joined with the interior Sverdrup transport. There is no proper separation of the western boundary current, and the NRG does not exist; the boundary of subpolar–subtropical gyre is farther north, determined purely by the wind stress curl. With W_B taken from the robust diagnostic calculation and no wind stress (Fig. 12b), the bottom vortex stretching alone is found to drive the horizontal gyres as strongly as the wind-driven circulations (which of course is not to say that the wind does not ultimately drive the gyres). The northern and southern recirculation exists on both sides of the Gulf Stream, and the western boundary current separates from the coast a little south of Cape Hatteras. The result clearly shows the impact of the DWBC on the subpolar–subtropical gyre circulation. With both surface wind stress and bottom vortex stretching taken from the robust diagnostic calculation (Fig. 12c), equivalent to the sum of the results in Figs. 12a and 12b, the western boundary current separates at the right place, and the Sverdrup theory breaks down in the interior ocean. Here the NRG is stronger than that calculated from the full three-dimensional OGCM (Fig. 2b). The existence of the anticyclonic southern recirculation in Figs. 12b and 12c, as shown in Fig. 2b, indicates that the southern recirculation is also related to bottom upwelling induced by upslope bottom flow over the bottom seamount there, which produces negative vorticity.

Figures 12d,e,f show the cases with both surface wind forcing and bottom vortex stretching taken from the prognostic experiments. Again, there is a relatively strong NRG in the control run, both experiment I and the path of the western boundary current downstream of Cape Hatteras shift to southern latitudes. The NAC also turns more northward to the east of the Grand Banks around 46°W, as indicated by the strong zonal gradient in the streamfunction around 43°N, 46°W. This is consistent with the three-dimensional prognostic modeling results (Fig. 11b), in which the stronger southward DWBC near the Grand Banks is associated with stronger northward offshore NAC. In the simple barotropic model, the strong zonal gradient in the streamfunction around 43°N, 46°W is due to strong bottom downwelling induced by the downslope DWBC there, suggesting that the bottom vortex stretching induced by the downslope DWBC east of the Grand Banks contributes to the enhancement of northward offshore NAC. With higher viscosity (Fig. 12e) or weaker DWBC (Fig. 12f), the Gulf Stream path shifts northward, the NRG is much weaker or disappears, and the NAC moves more eastward.

Similarly, Fig. 13 shows the barotropic streamfunction for the cases with ECMWF AMIP II and the high-resolution satellite-observed QuikSCAT surface wind stress. With only ECMWF AMIP II climatological (1979–95) surface wind stress (Fig. 13a), the solution is similar to that in Fig. 12a, that is, the Munk boundary layer joins with the interior Sverdrup transport. There is no proper separation of the western boundary current and the NRG does not exist. Here the boundary of subpolar–subtropical gyre shifts to 45°N, and the subpolar gyre is much stronger, resulting from the strong

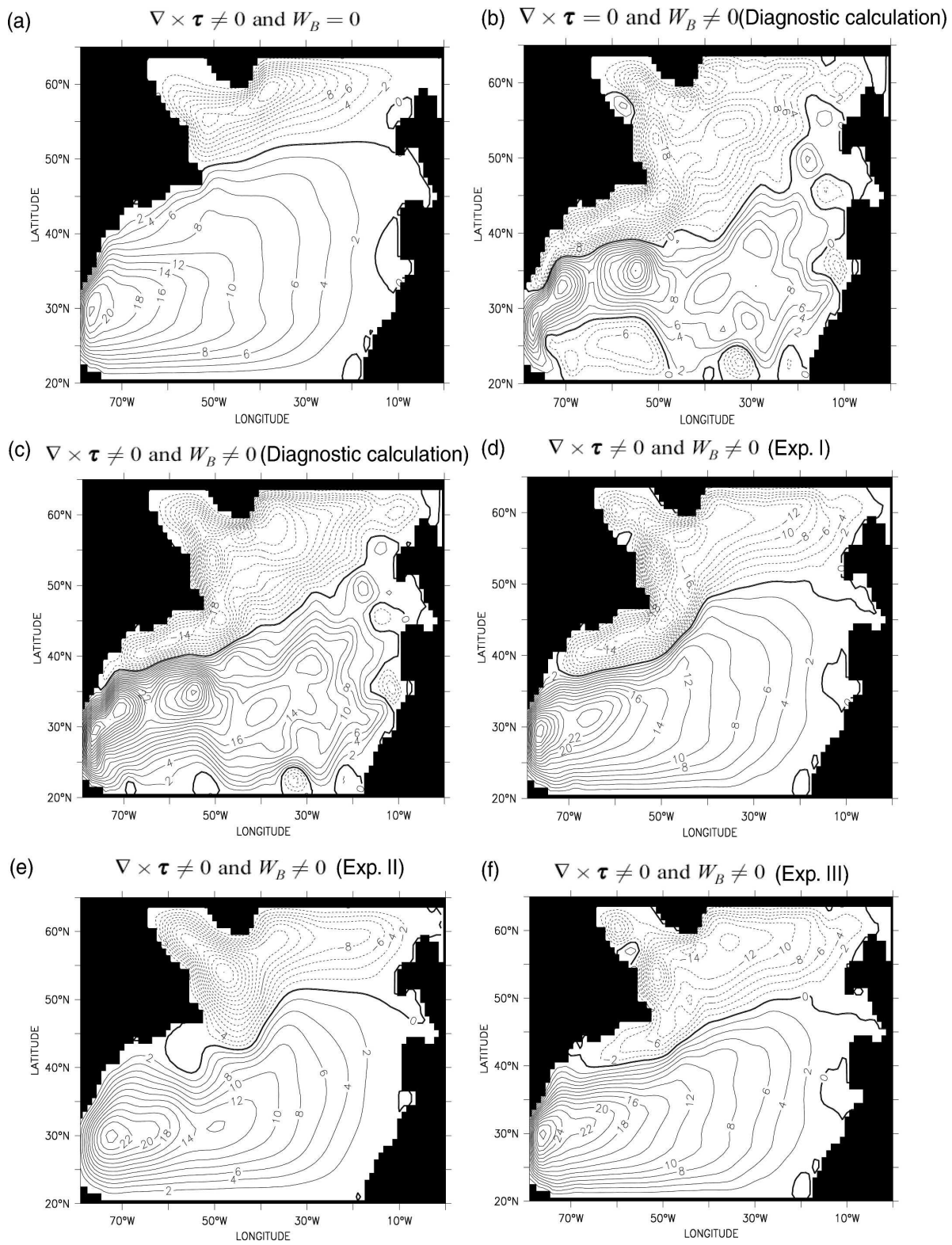

FIG. 12. Barotropic streamfunction calculated from the simple barotropic model using COADS wind stress: (a) $\nabla \times \boldsymbol{\tau} \neq 0$ and $W_B = 0$; (b) $\nabla \times \boldsymbol{\tau} = 0$ and $W_B \neq 0$, W_B is from the robust diagnostic calculation; (c) $\nabla \times \boldsymbol{\tau} \neq 0$ and $W_B \neq 0$, W_B is from the robust diagnostic calculation; (d) $\nabla \times \boldsymbol{\tau} \neq 0$ and $W_B \neq 0$, W_B is from experiment I, control run; (e) $\nabla \times \boldsymbol{\tau} \neq 0$ and $W_B \neq 0$, W_B is from experiment II, higher lateral viscosity; and (f) $\nabla \times \boldsymbol{\tau} \neq 0$ and $W_B \neq 0$, W_B is from experiment III, weaker DWBC.

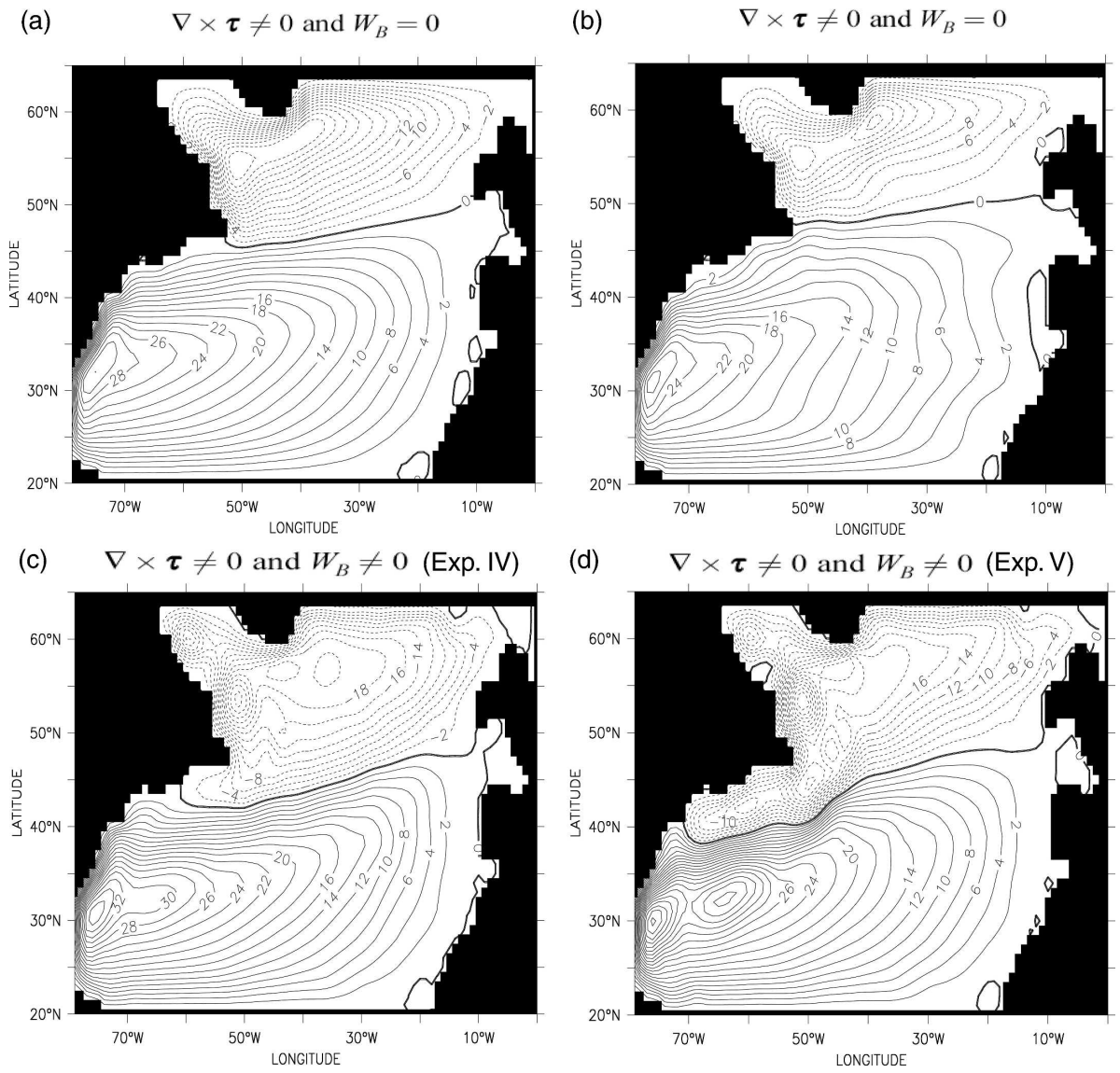

FIG. 13. Barotropic streamfunction calculated from the simple barotropic model using ECMWF AMIP II and QuikSCAT wind stress: (a) $\nabla \times \boldsymbol{\tau} \neq 0$ and $W_B = 0$, $\boldsymbol{\tau}$ is ECMWF AMIP II 1979–95 climatological wind stress; (b) $\nabla \times \boldsymbol{\tau} \neq 0$ and $W_B = 0$, $\boldsymbol{\tau}$ is QuikSCAT 4-yr (from August 1999 to July 2003) climatological wind stress; (c) $\nabla \times \boldsymbol{\tau} \neq 0$ and $W_B \neq 0$, $\boldsymbol{\tau}$ is ECMWF climatology wind stress, W_B is from experiment IV, ECMWF AMIP II wind stress and weak wind speed; and (d) $\nabla \times \boldsymbol{\tau} \neq 0$ and $W_B \neq 0$, $\boldsymbol{\tau}$ is ECMWF AMIP II 1979–95 climatological wind stress, W_B is from experiment V, ECMWF AMIP II wind stress and COADS wind speed.

positive wind stress curl in the subpolar region. With only the high-resolution satellite-observed QuikSCAT surface wind stress (climatology from August 1999 to July 2003), which has very strong positive wind stress curl to the north of the Gulf Stream, the results (Fig. 13 b) are also very similar to that in (Fig. 13a). Here, too, there is no proper separation of the western boundary current and the NRG does not exist, and the boundary of the subpolar–subtropical gyre near the western coast is close to 48°N. We also did the calculation with only the annual mean ECMWF operational surface wind stress (ECMWF 1989) of 1986, which has very strong positive wind stress curl at the north of Gulf Stream, similar to that shown in Gangopadhyay and Chao (2000). The result is very similar to Fig. 13b, and again there is no proper separation and the NRG does not exist. Although there is strong positive wind stress curl at the north of Gulf Stream in each of the wind products mentioned above, the negative wind stress curl at the eastern North Atlantic region at similar latitudes is also very strong and extensive. What matters to the subpolar–subtropical gyre boundary near the western

boundary is the zero line of the integrated Sverdrup transport across the basin, not just the local wind vorticity (Rhines and Schopp 1991; Böning et al. 1991). The results show that strong positive wind stress curl at the north of the Gulf Stream cannot lead to the formation of the NRG and the separated path of the western boundary current downstream of Cape Hatteras alone. With both ECMWF AMIP II wind stress and bottom vortex stretching taken from experiment IV (Fig. 13c), the path of the western boundary current is farther north because of the weak bottom vortex stretching associated with a weak DWBC. With both ECMWF AMIP II wind stress and bottom vortex stretching taken from experiment V (Fig. 13d), the much stronger bottom vortex stretching leads to the formation of NRG and the path of the western boundary current shifts to the south, similar to that in Fig. 12d.

In our full prognostic three-dimensional model, we found that the strength of cyclonic NRG at north of the Gulf Stream is much stronger and the Gulf Stream path downstream of Cape Hatteras shifts to southern latitudes when the DWBC is relatively stronger at south of the Grand Banks, that is, in experiments I and V as compared to experiments II, III, and IV. In the simple barotropic model that is just forced by the surface wind stress and W_B, we found very similar results as those of the prognostic GCM experiments: the strength of the cyclonic NRG at north of the Gulf Stream is much stronger and the path of the western boundary current downstream of Cape Hatteras shifts to a southern latitude for the cases forced with W_B from the prognostic GCM experiments I and V (Figs. 12d, 13d), compared to the cases forced with W_B from the prognostic GCM experiments II, III, and IV (Figs. 12e,f, 13c). This is consistent with stronger bottom downwelling at the western boundary near the Grand Banks in experiments I and V (Fig. 9 a).

As we expect from the scaling, the path of the depth-integrated western boundary current and the formation of NRG are very sensitive to the magnitude of bottom vortex stretching induced by downslope bottom currents, but are not particularly sensitive to the difference of surface wind stress curl between COADS and ECMWF AMIP II wind stress.

7. An analytical solution

In this section, we find an analytical solution of for the vertically integrated flow, using the model presented in section 4. In particular, we solve for the vertically integrated streamfunction for both the interior ocean and the vicinity of the western boundary for a given vertical velocity at the ocean bottom, chosen to mimic the effects of flow over the continental slope.

a. The interior ocean: The cyclonic NRG and the path of the western boundary current

In the interior ocean, the viscous term can be ignored, and (4.1) becomes

$$\beta \frac{\partial \Psi}{\partial x} = \frac{1}{\rho_0} \mathbf{k} \cdot \boldsymbol{\nabla} \times \boldsymbol{\tau} - f_0 W_B. \tag{7.1}$$

Given the no-normal flow condition at the eastern boundary condition, we integrate the above equation from the eastern boundary and obtain the solution in the interior ocean:

$$\Psi_I + \Psi_S + \Psi_{\mathrm{WI}} = -\frac{1}{\beta} \int_x^{x_E} \left(\frac{\mathbf{k} \cdot \boldsymbol{\nabla} \times \boldsymbol{\tau}}{\rho_0} - f_0 W_B \right) dx', \tag{7.2}$$

where Ψ_I is the total interior transport, which is the sum of the Sverdrup transport Ψ_S and the transport induced by interior bottom vortex stretching Ψ_{WI}. Conventional Sverdrup theory of interior transport breaks down whenever the interior bottom vortex stretching is on the same order or larger than the forcing of surface wind stress curl. Here "interior" means away from the vicinity of surface western boundary at each latitude. In the robust diagnostic calculation and experiments I and V (Fig. 9), significant interior bottom downwelling appears at the western boundary near Grand Banks, resulting in $\Psi_{\mathrm{WI}} < 0$ and contributing to the cyclonic NRG there; significant interior bottom upwelling appears in the robust diagnostic calculation over the bottom seamount (35°N, 52°), resulting in $\Psi_{\mathrm{WI}} > 0$ and contributing to the anticyclonic southern recirculation gyre. The position of the subpolar–subtropical boundary at the interior ocean is determined by the relationship $\Psi_I = \Psi_S + \Psi_{\mathrm{WI}} = 0$. Without the interior bottom vortex stretching, the path of the depth-integrated western boundary current, which is also the boundary of the subpolar–subtropical gyre in the western North Atlantic, is located at the zero line of the Sverdrup transport, that is, $\Psi_S = 0$. With any realistic surface wind stress, $\Psi_S > 0$ south of the boundary, and $\Psi_S < 0$ north of the boundary, that is, $\partial \Psi_S / \partial y < 0$. With a large enough interior bottom downwelling ($W_B < 0$, thus $\Psi_{\mathrm{WI}} < 0$) near the south of the Grand Banks, the path of the depth-integrated western boundary current (where $\Psi_I = 0$) is shifted to the south ($\Psi_S > 0$) and the cyclonic NRG ($\Psi_I < 0$) is formed at the north of the Gulf Stream.

In our prognostic experiment I, the modeled bottom vortex stretching is able to counter the wind-driven

Sverdrup transport south of the Grand Banks, and thus the modeled barotropic streamfunction shows a cyclonic NRG, which makes the boundary between the subpolar and subtropical gyre (i.e., the axis of the depth-integrated western boundary current) downstream of Cape Hatteras, shifted south from the latitude it would have if it was purely wind driven.

b. Solution in the vicinity of the western boundary

Near the western boundary, the wind stress curl can be ignored, and Eq. (4.1) becomes

$$\beta \frac{\partial \Psi}{\partial x} = A_H \nabla^4 \Psi - f_0 W_B. \tag{7.3}$$

The analytical barotropic model is similar to that in Gangopadhyay and Chao (2000), but here we include a nonzero W_B near the western boundary. The solutions obviously depend on the specification of W_B; let us assume that W_B in the vicinity of the western boundary has a damped oscillatory zonal profile in order to represent the interaction of the bottom boundary current with the continental slope. Thus, let

$$W_B = W_{\mathrm{BB}}(y) \exp(-px/\delta_M) \sin(qx/\delta_M), \tag{7.4}$$

where $\delta_M = (A_H/\beta)^{1/3}$ is the Munk layer scale and $|W_{\mathrm{BB}}(y)|$ represents the amplitude of W_B in the vicinity of the western boundary. The assumed profile of W_B is just a convenient form to describe the bottom vertical velocity in the vicinity of the western boundary. It has the following two characteristics. First, it decays rapidly into the interior, and this enables an analytic asymptotic boundary layer approach to be used to assess its role. Because W_B in the vicinity of the western boundary is induced by the flow over a steep continental slope, its amplitude would decay away from the steep continental slope; hence, δ_m/p represents the zonal exponentially decaying scale of W_B near the western boundary that is affected by the width of the topographic slope. Second, it has an oscillatory structure, representing the zonal wave-like structure of the bottom vertical velocity near the boundary that is seen in our robust diagnostic calculation. The oscillatory scale is given by δ_m/q, which is also affected by the width of the topographic slope, that is, a narrower topographic slope will lead to a smaller scale. The profile of W_B from the robust diagnostic calculation at 36°N in the western North Atlantic, near the Gulf Stream separation point, is plotted in Fig. 14a. It shows an oscillatory structure and approximately exponentially decay amplitude of W_B near the western boundary (west of 65°W), similar to our assumed zonal profile of W_B in the vicinity of the western boundary with $p \approx 0.4$ and $q \approx 0.6$. In Fig. 14a the W_B at the east of 65°W is the interior bottom vertical velocity that contributes to the Ψ_{WI} discussed in section 7a. For example, the upwelling near 52°W is induced by an upslope bottom flow over the interior seamount near 52°W, and contributes to the anticyclonic southern recirculation gyre centered at 35°N, 55°W (Fig. 2b).

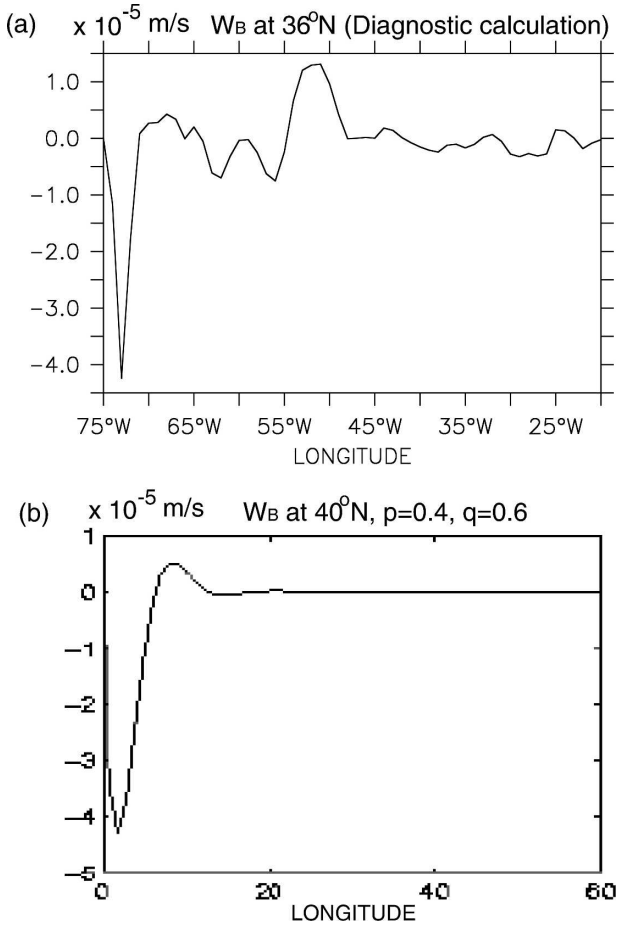

FIG. 14. Zonal profile of W_B.: (a) along 36°N from the robust diagnostic calculation and (b) at 40°N [the latitude with the maximum $|W_{\mathrm{BB}}(y)|$] used for the analytical solution with $p = 0.4$ and $q = 0.6$.

The western boundary current separation point is determined by the no-stress condition ($\Psi''|_{x=0} = 0$) at the western boundary. The details are discussed in appendix B. Without the bottom vortex stretching, the western boundary current separates (as expected) at the point where the Sverdrup transport vanishes at the western boundary, that is, $\Psi_S|_{x=0} = 0$. However, if the bottom vortex stretching is sufficiently large the western boundary current can separate at a more southern

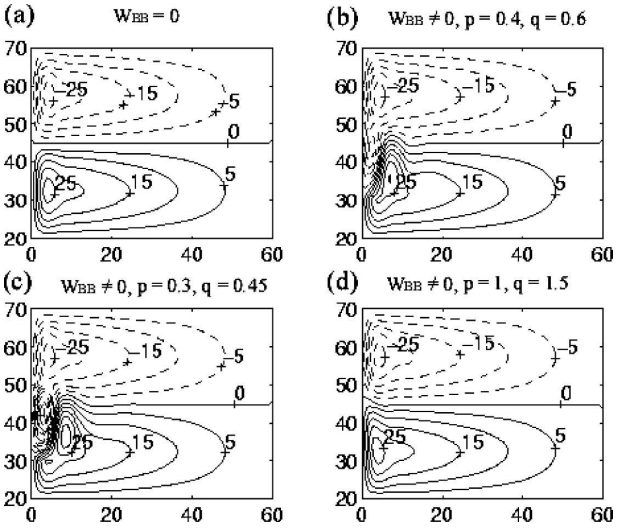

FIG. 15. Analytical solution of the barotropic streamfunction solved in appendix B [Eqs. (B.2), (B.3), and (B.4)]; (a) $W_{BB}(y) = 0$ (wind forcing only); (b) $W_{BB}(y) \neq 0$ (bottom vortex stretching included), $p = 0.4$ and $q = 0.6$; (c) $W_{BB}(y) \neq 0$ (bottom vortex stretching included), $p = 0.3$ and $q = 0.45$ (wider zonal scale of W_B); and (d) $W_{BB}(y) \neq 0$ (bottom vortex stretching included), $p = 1$ and $q = 1.5$ (narrower zonal scale of W_B).

latitude ($\Psi_S|_{x=0} > 0$), because of the bottom downwelling [$W_{BB}(y) < 0$] near the western boundary or the bottom downwelling in the interior ocean ($\Psi_{WI}|_{x=0} < 0$) (appendix B).

c. *Examples of analytic solutions*

For simplicity we choose a wind stress $\boldsymbol{\tau}$ that has only a zonal component and that gives a double-gyre solution in a box domain from 20° to 70°N in latitude and 0° to 60°W in longitude; explicitly, $\tau^x = \tau_0 \cos[\pi(y - 45°)/25°]$, where $\tau_0 = 0.08$ N m^{-2} and y is the latitude in degrees. We choose the lateral viscosity to be the same as that used in our robust diagnostic calculations. Without any bottom vertical velocity, the barotropic streamfunction is just the Munk boundary layer solution joining the Sverdrup transport in the interior, which represents symmetric subtropical–subpolar double gyres (Fig. 15a). The western boundary current separates from the boundary at 45°, as predicted by the pure wind-driven circulation theory, that is, $\Psi_S|_{x=0}$.

When we include the effects of flow over the slope, the solution is much modified. For example, we specify $W_{BB}(y) = W_0 \sin[\pi(y - 50°)/20°]$ for $30° \leq y \leq 50°$, and $W_{BB}(y) = 0$ for $y > 50°$ and $y < 30°$ (here $W_0 = 1 \times 10^{-4}$ m s^{-1}). For the case with $p = 0.4$ and $q = 0.6$, W_B (Fig. 14b) has the same zonal exponentially decaying and oscillatory scales as that in the robust diagnostic calculation (Fig. 14a). In this case (Fig. 15b), the subpolar gyre extends southward near the western boundary and the cyclonic recirculation in the vicinity of the western boundary forms at the south of the zero wind stress curl line. The western boundary current separates from the boundary near 33°, farther south than that predicted by the pure wind-driven circulation theory ($\Psi_S|_{x=0}$) as predicted by Eq. (B8) in appendix B. For this simple box domain, we do not include any interior bottom downwelling, that is, $\Psi_{WI} = 0$.

With a wider scale of continental slope (wider zonal scales of W_B) compared to the Munk layer scale, that is, $p = 0.3$ and $q = 0.45$ (Fig. 15c), the bottom vortex-stretching term dominates the western boundary, and the cyclonic recirculation induced by the bottom downwelling in the vicinity of the western boundary is stronger. With the narrower scale of the continental slope (narrower zonal scales of W_B) relative to the Munk layer scale, that is, $p = 1$ and $q = 1.5$ (Fig. 15d), the bottom vortex-stretching term has no impact on the wind-driven symmetric double gyre, and the Munk boundary layer will dominate the solution. (In the real ocean, the width of the topographic slope near the Gulf Stream separation region is larger than the Munk layer scale.)

The mechanisms of the contribution of bottom downwelling to both the separation of the depth-integrated western boundary current near Cape Hatteras and the formation of the NRG associated with the separated path of the depth-integrated western boundary current in the interior ocean are summarized in the schematic diagram (Fig. 16). With a higher lateral viscosity, the deep current would be weaker and diffused to the interior ocean, and the separation pattern would be improperly simulated.

8. Summary and discussion

Both the simple theory and numerical results suggest that the presence of the NRG and the separated path of the depth-integrated western boundary current downstream of Cape Hatteras are affected by the presence of a DWBC south of the Grand Banks. Given a reasonable DWBC, it is possible for a model with relatively coarse resolution, namely, 1°, to give a separated path of depth-integrated western boundary current downstream of Cape Hatteras and a cyclonic NRG. In contrast to the importance of the DWBC, both our prognostic coupled model and the simple barotropic model show that the strong positive wind stress curl north of Gulf Stream does not of itself lead to the formation of a NRG and a properly separated western boundary current, although it may help to reduce the unrealistic anticyclonic eddy north of Cape Hatteras found in some

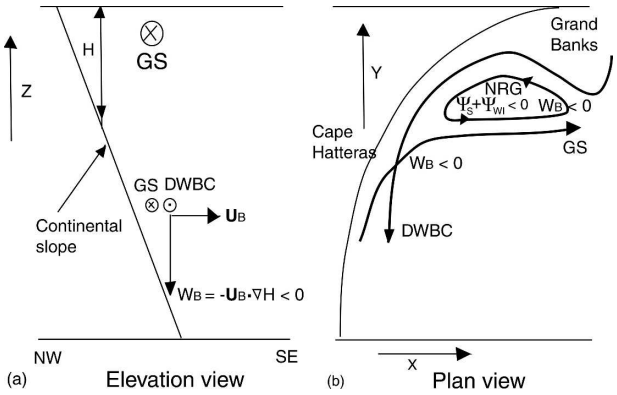

FIG. 16. Schematic diagram of the contribution of bottom downwelling. (a) Elevation view. A vertical section across the topographic isobath near Cape Hatteras. At deeper ocean, the DWBC begins to move downslope when it meets the Gulf Stream (GS) at the same depth and induces strong bottom downwelling ($W_B < 0$). (b) Plan view. The bottom downwelling ($W_B < 0$) at the crossover of the GS and DWBC contributes to the separation of the depth-integrated western boundary current from Cape Hatteras, and the bottom downwelling ($W_B < 0$) near the southwest of the Grand Banks contributes to the formation of the cyclonic NRG, and keeps the path of the depth-integrated western boundary current downstream of Cape Hatteras separated from the coast.

eddy-permitting models (Chao et al. 1996; Gangopadhyay and Chao 2000).

There are no mesoscale dynamics resolved by our model configuration. The modeled Gulf Stream width is similar to previous modeling results, with 1° horizontal resolution (Gerdes and Köberle 1995), and is perforce much wider than that observed. Dengg et al. (1996) pointed out that models with 1° horizontal resolution should still be able to resolve the NRG, and so the simulation should ideally produce a depth-integrated western boundary current that is no longer attached to the shelf in this region. Our modeling results are consistent with this; that is, the model is able to generate the NRG when the DWBC is strong enough, and the modeled path of depth-integrated western boundary current downstream of Cape Hatteras is then not attached to the shelf. Similar results are found in a recent study using the coupled National Center for Atmospheric Research (NCAR) Parallel Climate Model (PCM) with ⅔° horizontal resolution in the OGCM, which the separated Gulf Stream path moves with the strength of the DWBC (Dai et al. 2005).

Strong bottom downwelling induced by a downslope DWBC also appears at the crossover of the DWBC and the Gulf Stream near Cape Hatteras in those of our numerical experiments that do have a strong DWBC, and especially in the robust diagnostic calculation. This feature has been found not only in our numerical models, but also in observations (Pickart and Watts 1990; Pickart and Smethie 1993; Lindstrom and Watts 1994; Bower and Hunt 2000). Simple scaling arguments suggest that vortex stretching resulting from flow across bathymetry is a leading term in the vertically integrated vorticity equation near the Gulf Stream separation point. Our analytical model and the simple numerical barotropic model forced with bottom downwelling from the robust diagnostic calculation suggest that bottom vortex stretching at the crossover contributes to the separation of the depth-integrated western boundary current at Cape Hatteras. Our analytical model also shows that with a continental slope that is wider than the Munk layer scale, the bottom vortex stretching is a dominant term in the dynamics of the western boundary, as also noted by Hughes and De Cuevas (2001).

The bottom vortex stretching is, in fact, important over an extended area in the North Atlantic, and our simple numerical barotropic model for the robust diagnostic calculation case shows that its contribution to the North Atlantic subpolar and subtropical gyres is on the same order as that of the surface wind stress curl. The implied inaccuracy of Sverdrup balance is generally consistent with the observational study of Wunsch and Roemmich (1985); they estimated that in the eastern North Atlantic, a horizontal deep flow of 0.1 cm s^{-1} (resulting from large-scale thermohaline flows or mesoscale eddies at the deep ocean) would be enough to generate a vertical bottom velocity larger than that of the surface wind-driven Ekman velocity over the topographic slope associated with the Mid-Atlantic Ridge. Similarly, Greatbatch et al. (1991) show that the North Atlantic barotropic transport driven by the bottom pressure torque is stronger than the wind-driven circulation in many areas in the basin, and Holland and Hirschman (1972) consistently found that it is the interaction of deep flow with bottom topography that makes the barotropic streamfunction different from, and in places stronger than, the Sverdrup transport.

Our results suggest that at least part of the difficulty that many OGCMs have in producing the cyclonic NRG and a properly separated Gulf Stream is that their DWBC in the region from Cape Hatteras to the Grand Banks is not strong enough, even though their total thermohaline circulation strength may be similar to that of the observations. Indeed, many modeled deep currents move southward in the interior ocean (unrealistically) instead of along the western boundary in midlatitudes from 30° to 50°N, that is, in the region from Cape Hatteras to the Grand Banks. Even if the modeled deep overflow through the Denmark Strait were as strong as that observed (Döscher et al. 1994), part of the downstream deep currents may move southward in

the interior ocean and the DWBC may not be strong enough in the region from Cape Hatteras to the Grand Banks. Semtner and Chervin (1992) found that the modeled deep circulation of the North Atlantic does not show a very well-defined boundary flow between 30° and 50°N in a ½° OGCM simulation; the DWBC moves northward off the Grand Banks instead of moving southward as observed, and the southward deep current at these latitudes spread into interior ocean near 30° and 24°W.

Similarly, in the model simulations of CFC uptake in North Atlantic Deep Water using a ⅓° OGCM (Beismann and Redler 2003), the DWBC signal is found in the interior of the basin instead of close to the continental shelf near the Grand Banks. They found that even at a higher resolution (⅓°), the simulated southward deep current is not close to the continental slope around the southern tip of the Grand Banks, but rather takes a path along the western slope of the Mid-Atlantic Ridge before it turns west at about 40°N; the spreading rate in this region is about the same as that in the ⅓° and ⅔° experiments, and only south of about 35°N is the DWBC signal found to be stronger in the ⅓° model. Higher-resolution models do not necessarily have stronger thermohaline circulation (THC), because of the strong sensitivity of THC to surface and northern boundary conditions. For example, Beckmann et al. (1994) found that the strength of the THC is weakened and there is no significant improvement in the modeled NRG and Gulf Stream path in a ⅙° simulation, compared to their ⅓° simulation.

Some high-resolution models do have a good separation and realistic path of the Gulf Stream, for example, the 0.1° eddy-resolving simulation of Smith et al. (2000). In this simulation the bottom downwelling induced by the downslope DWBC both south of Grand Banks and at the crossover near Cape Hatteras is quite strong and significantly larger than the contribution from surface wind stress curl, and it is the leading term in the vertically integrated vorticity equation (R. Smith 2003, personal communication). A recent eddy-resolving modeling study (Bryan et al. 2007) also suggests that the DWBC plays a significant role in the Gulf Stream separation at Cape Hatteras. In our model, the use of an EBM is particularly helpful in proving the proper surface fluxes that lead to relatively strong Labrador Sea deep convection and strong DWBC.

We emphasize that we have not provided a complete theory of the path of the depth-integrated western boundary current; for example, eddying and inertial effects are absent. Rather, we are only suggesting that the flow over the continental slope can provide a forcing that is locally as important as the wind stress curl in determining the path of the depth-integrated western boundary current. This suggestion is supported by a number of numerical simulations, scaling theory, and semianalytic models, although one would require a suite of experiments with a stratified, high-resolution model to be wholly definitive. Also, we do not predict the latitude of separation. Rather, we have simply tried to point out the importance of the DWBC, and elucidate the mechanism whereby it contributes to the formation of the NRG and the path of the depth-integrated western boundary current.

Acknowledgments. We thank Kirk Bryan for helpful discussions; Isaac Held for providing us the EBM; Mike Winton, Steve Griffies, and Matt Harrison for the help with MOM4 and the coupled model; and Gabriel Vecchi for providing us the ECMWF operational wind. The numerical experiments were carried with the supercomputer facilities at GFDL. The work was partially funded by NSF under Grant OCE 0351383.

APPENDIX A

Description of the Coupled Model

We developed a simple global coupled model within the Geophysical Fluid Dynamics Laboratory (GFDL) Flexible Modeling System (FMS) framework. We coupled a two-dimensional global atmospheric EBM with hydrological cycle to a global OGCM (GFDL MOM4; Griffies et al. 2004) and a slab sea ice model (Winton 2000). The EBM solves for atmospheric temperature and specific humidity. The atmospheric temperature is governed by the balance of shortwave radiation absorption (Q_{SWa}), upward longwave radiation at the top of the atmosphere (Q_{LWut}), surface downward and upward longwave radiation (Q_{LWds}, Q_{LWus}), upward surface sensible heat flux (Q_{SH}), latent heat flux released during precipitation (Q_{LH}), and lateral eddy diffusion. The specific humidity is governed by the balance of evaporation (E), atmospheric precipitation (P), and lateral eddy diffusion. The lateral eddy diffusion coefficient κ is 10^6 m^2 s^{-1}. Typical EBMs have no horizontal advection of temperature and specific humidity, and the resulting hydrological cycle would be quite different from observations. Hence, we include advection terms (A_T, A_q) diagnosed from observations [the Ocean Model Intercomparison Project (OMIP) dataset; Röske 2001] for temperature and specific humidity, respectively, so that the resulting hydrological cycle and surface air temperature are similar to those of the observations. The EBM equations for atmospheric

temperature T and specific humidity q are summarized here:

$$C_A \frac{\partial T}{\partial t} = Q_{\mathrm{SWa}} + Q_{\mathrm{LWus}} - Q_{\mathrm{LWds}} - Q_{\mathrm{LWut}} + Q_{\mathrm{LH}} + Q_{\mathrm{SH}} + C_A \kappa \nabla^2 T - C_A A_T \quad \text{and} \tag{A.1}$$

$$\frac{\partial q}{\partial t} = \frac{E - P}{h} + \kappa \nabla^2 q - A_q, \tag{A.2}$$

where C_A is the heat capacity of the atmospheric column (8×10^6 J m^{-2} K^{-1}), and $h = 8$ km is the atmospheric height.

The shortwave radiation absorption is given by $Q_{\mathrm{SWa}} = a_{\mathrm{abs}} S_0 \gamma(y, t)$. Here a_{abs} is the solar radiation absorption coefficient, $S_0 = 1360$ W m^{-2} is the solar constant, and $\gamma(y, t)$ is the distribution of the incoming solar radiation as a function of latitude y and time t. The longwave radiations are calculated with the blackbody law. The surface sensible heat flux and evaporation over the ocean are calculated with the bulk formula. Over land, we specified the surface heat flux and evaporation using the OMIP climatological dataset. The precipitation occurs when the relative humidity is greater than a threshold. The EBM extended globally and has T42 horizontal resolution. The OGCM (MOM4) extended from 80° to 90°S, with a tripolar grid (Murray 1996) and realistic bathymetry. It has 1° × 1° resolution in the horizontal and 20 levels in vertical varying from 50 m at surface to 600 m at depth. The OGCM has an explicit free surface, employing the K-profile parameterization (KPP) (Large et al. 1994), the Gent–McWilliams (GM) scheme (Gent and Mc Williams 1990), full convection scheme (Rahmstorf 1993), and background Bryan–Lewis vertical diffusivity (Bryan and Lewis 1979). The Bering Strait is closed and the Mediterranean Sea is not included. The surface freshwater flux is represented as a virtual salt flux. The sea ice model has the same domain and horizontal resolution as that of the OGCM. The model is forced with external surface wind stress and surface wind speed and spun up together with the atmosphere, ocean, and sea ice, exchanging information once a day.

APPENDIX B

Analytical Solution

We solve the vertically integrated vorticity equation analytically near the western boundary as

$$\beta \frac{\partial \Psi}{\partial x} = A_H \nabla^4 \Psi - f_0 W_{\mathrm{BB}}(y) \exp(-px/\delta_M) \sin(qx/\delta_M), \tag{B.1}$$

with the boundary conditions $\Psi|_{x=0} = 0$, $\Psi'|_{x=0} = 0$ (no slip) and $\Psi_{x/\delta_{M\to\infty}} = \Psi_I$. The solution in the vicinity of the western boundary is

$$\Psi = \Psi_M + \Psi_{\mathrm{WB}}, \tag{B.2}$$

where Ψ_M is the Munk boundary layer solution and Ψ_{WB} is the boundary layer solution induced by bottom vortex stretching within the boundary layer. Let $\xi = x/\delta_M$, and we have

$$\Psi_M = \Psi_I \left[1 - \frac{\sqrt{3}}{3} \exp\left(-\frac{\xi}{2} \right) \sin\left(\frac{\sqrt{3}}{2} \xi \right) - \exp\left(-\frac{\xi}{2} \right) \cos\left(\frac{\sqrt{3}}{2} \xi \right) \right] \tag{B.3}$$

(notice that here $\Psi_I = \Psi_S + \Psi_{\mathrm{WI}}$ as discussed in section 7a) and

$$\Psi_{\mathrm{WB}} = \frac{f_0 W_{\mathrm{BB}}(y) \delta_M}{\beta R_1} \left[\exp(-p\xi) \sin(q\xi + \phi) + c_1 \exp\left(-\frac{\xi}{2} \right) \sin\left(\frac{\sqrt{3}}{2} \xi \right) + c_2 \exp\left(-\frac{\xi}{2} \right) \cos\left(\frac{\sqrt{3}}{2} \xi \right) \right], \tag{B.4}$$

where $R_1 = \{[q(1 + 4p^3 - 4pq^2)]^2 + (p + p^4 - 6p^2q^2 + q^4)^2\}^{1/2}$, $c_1 = (\sqrt{3}/3)[(2p - 1)\sin\phi - 2q\cos\phi]$, $c_2 = -\sin\phi$, and $\phi = \arctan[q(1 + 4p^3 - 4pq^2)/(p + p^4 - 6p^2q^2 + q^4)]$.

The western boundary current separation point is determined by the no-stress condition at the western boundary, that is,

$$\Psi''|_{x=0} = \Psi''_M|_{x=0} + \Psi''_{\mathrm{WB}}|_{x=0} = 0. \tag{B.5}$$

Based on the solution in the vicinity of the western boundary [Eqs. (B.2), (B.3), and (B.4)], we have

$$\Psi''_M|_{x=0} = \Psi_{\mathrm{I}}|_{x=0} = \Psi_S|_{x=0} + \Psi_{\mathrm{WI}}|_{x=0} \quad \text{and} \tag{B.6}$$

$$\Psi''_{\mathrm{WB}}|_{x=0} = \frac{f_0 W_{\mathrm{BB}}(y) \delta_M R_2}{\beta R_1} \sin(\phi + \alpha), \tag{B.7}$$

where $R_2 = \sqrt{[(2p - 1)q]^2 + (q^2 - p^2 + p - 1)^2}$, and $\alpha = \arctan(2p - 1)q/(q^2 - p^2 + p - 1)$. The latitude at which the west boundary current separates from the coast is then determined by the relationship

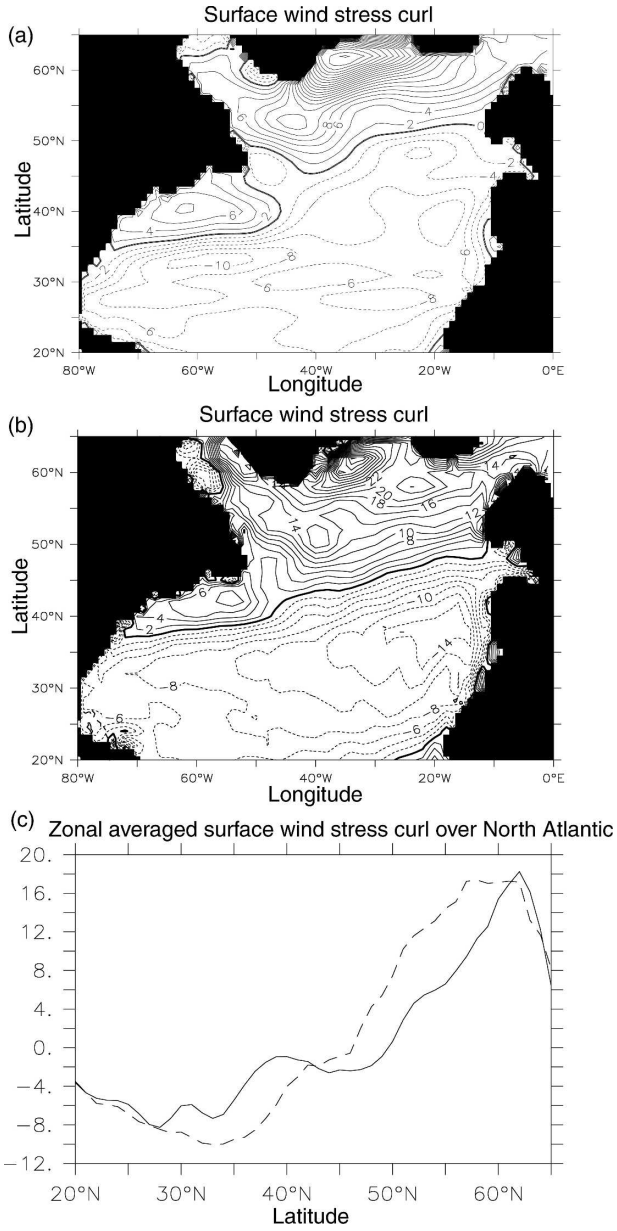

FIG. C1. Annual mean COADS and ECMWF AMIP II climatological wind stress curl (unit is 10^{-8} N m^{-3}): (a) COADS climatological wind stress curl over the North Atlantic Ocean, (b) ECMWF AMIP II 1979–95 climatological wind stress curl over the North Atlantic Ocean, and (c) zonally averaged COADS (solid line) and ECMWF AMIP II 1979–95 (dashed line) climatological wind stress curl over the North Atlantic Ocean.

$$\Psi_S|_{x=0} + \Psi_{\mathrm{WI}}|_{x=0} + \frac{f_0 W_{\mathrm{BB}}(y)\delta_M R_2}{\beta R_1}\sin(\phi + \alpha) = 0. \tag{B.8}$$

For small enough p and q, we have $\sin(\phi + \alpha) > 0$. The analytical solution of the barotropic streamfunction [Eqs. (B.2), (B.3), and (B.4)] is plotted in Fig. 15.

APPENDIX C

Description of Surface Wind Stress

In our prognostic experiments, we use two different surface wind stress datasets: the COADS climatological wind stress (Da Silva et al. 1994), and the 1979–95 climatological surface wind from the AMIP II integration (Gates 1992) with the ECMWF operational model (ECMWF 1991). We plot the two-dimensional distribution and zonal average of COADS and ECMWF AMIP II climatological wind stress curl over the North Atlantic Ocean (Fig. C1). The ECMWF AMIP II climatological wind stress curl is stronger than that of COADS in both the subpolar and subtropical gyres (Fig. C1c). The ECMWF AMIP II wind-driven barotropic streamfunction (Fig. 13a) shows that the subpolar–subtropical gyre boundary shifts to a southern latitude (45°N) compared to that (50°N) with the COADS wind stress (Fig. 12a), because the latitude of zero zonally averaged ECMWF AMIP II wind stress curl shifts to 45°N (Fig. C1c); however, the cyclonic NRG does not exist, and the western boundary current stays attached to the coast from Cape Hatteras all the way to Newfoundland (Fig. 13a). On the other hand, although the prognostic experiments I and V are forced with these two very different wind stresses (COADS and ECMWF AMIP II), respectively, they both obtain a similar cyclonic NRG and a separated path of the depth-integrated western boundary current downstream of Cape Hatteras (Figs. 3b, 7b) because the DWBC near the south of the Grand Banks in both experiments is relatively stronger than other prognostic experiments (Fig. 10a).

REFERENCES

Beckmann, A., C. W. Böning, C. Koberle, and J. Willebrand, 1994: Effect of increased horizontal resolution in a simulation of the North Atlantic Ocean. *J. Phys. Oceanogr.,* **24,** 326–344.

Beismann, J.-O., and R. Redler, 2003: Model simulations of CFC uptake in North Atlantic Deep Water: Effects of parameterizations and grid resolution. *J. Geophys. Res.,* **108,** 3159, doi:10.1029/2001JC001253.

Böning, C. W., R. Döscher, and H. J. Isemer, 1991: Monthly mean wind stress and Sverdrup transports in the North Atlantic: A comparison of the Hellerman–Rosenstein and Isemer–Hasse climatologies. *J. Phys. Oceanogr.,* **21,** 221–235.

Bower, A. S., and H. D. Hunt, 2000: Lagrangian observations of the deep western boundary current in the North Atlantic Ocean. Part II: The Gulf Stream–deep western boundary current crossover. *J. Phys. Oceanogr.,* **30,** 784–804.

Bryan, F. O., M. W. Hecht, and R. D. Smith, 2007: Resolution convergence and sensitivity studies with North Atlantic Circulation Models. Part I: The western boundary current system. *Ocean Modell.,* **16,** 141–159.

Bryan, K., 1963: A numerical investigation of a nonlinear model of a wind-driven ocean. *J. Atmos. Sci.,* **20,** 594–606.

——, and L. J. Lewis, 1979: A water mass model of the world ocean. *J. Geophys. Res.,* **84,** 2503–2517.

Cessi, P., R. V. Condie, and W. R. Young, 1990: Dissipative dynamics of western boundary currents. *J. Mar. Res.,* **48,** 677–700.

Chao, Y., A. Gangopadliyay, P. Bryan, and W. R. Holland, 1996: Modeling the Gulf Stream system, how far from reality? *Geophys. Res. Lett.,* **23,** 3155–3158.

Chassignet, E. P., 1995: Vorticity dissipation by western boundary currents in the presence of outcropping layers. *J. Phys. Oceanogr.,* **25,** 242–255.

Dai, A. G., A. Hu, G. A. Meehl, W. M. Washington, and W. G. Strand, 2005: Atlantic thermohaline circulation in a coupled general circulation model: Unforced variations versus forced changes. *J. Climate,* **18,** 2990–3013.

Danabasoglu, G., J. C. McWilliams, and W. G. Large, 1996: Approach to equilibrium in accelerated global oceanic models. *J. Climate,* **9,** 1092–1110.

Da Silva, A., A. C. Young, and S. Levitus, 1994: *Algorithms and Procedures*. Vol. 1, *Atlas of Surface Marine Data 1994,* NOAA Atlas NESDIS 6, 83 pp.

Dengg, J., 1993: The problem of Gulf Stream separation: A barotropic approach. *J. Phys. Oceanogr.,* **23,** 2182–2200.

——, A. Beckmann, and R. Gerdes, 1996: The Gulf Stream separation problem. *The Warmwatersphere of the North Atlantic Ocean,* W. Krauss, Ed., Gebr. Borntraeger, 253–290.

Döscher, R., C. W. Böning, and P. Herrmann, 1994: Response of circulation and heat transport in the North Atlantic to changes in thermohaline forcing in northern latitudes: A model study. *J. Phys. Oceanogr.,* **24,** 2306–2320.

ECMWF, 1989: The description of the ECMWF/WCRP level III—A global atmospheric data archive. Tech. Attachment, 72 pp.

——, 1991: Development of the operational 31-level T213 version of the ECMWF forecast model. *ECMWF Newsletter,* No. 56, ECMWF, Reading, United Kingdom, 7–13.

Ezer, T., and G. L. Mellor, 1992: A numerical study of the variability and the separation of the Gulf Stream, induced by surface atmospheric forcing and lateral boundary flows. *J. Phys. Oceanogr.,* **22,** 660–682.

——, ——, and R. J. Greatbatch, 1995: On the interpentadal variability of the North Atlantic Ocean: Model simulated changes in transport, meridional heat flux and coastal sea level between 1955–1959 and 1970–1974. *J. Geophys. Res.,* **100,** 10 559–10 566.

Gangopadhyay, A., and Y. Chao, 2000: Sensitivity of the Gulf Stream path on the cyclonic wind stress curl. *Global Atmos. Ocean Syst.,* **7,** 151–178.

——, P. Cornillon, and D. R. Watts, 1992: A test of the Parsons–Veronis hypothesis on the separation of the Gulf Stream. *J. Phys. Oceanogr.,* **22,** 1286–1301.

Gates, W. L., 1992: AMIP: The Atmospheric Model Intercomparison Project. *Bull. Amer. Meteor. Soc.,* **73,** 1962–1970.

Gent, P. R., and J. C. McWilliams, 1990: Isopycnal mixing in ocean circulation models. *J. Phys. Oceanogr.,* **20,** 150–155.

Gerdes, R., and C. Köberle, 1995: On the influence of DSOW in a numerical model of the North Atlantic general circulation. *J. Phys. Oceanogr.,* **25,** 2624–2641.

——, A. Biastoch, and R. Redler, 2001: Fresh water balance of the Gulf Stream system in a regional model study. *Climate Dyn.,* **18,** 17–27.

Greatbatch, R. J., A. F. Fanning, A. D. Goulding, and S. Levitus, 1991: A diagnosis of interpendatal circulation changes in the North Atlantic. *J. Geophys. Res.,* **96,** 22 009–22 023.

Griffies, S. M., M. J. Harrison, R. C. Pacanowski, and A. Rosati, 2004: A technical guide to MOM4. NOAA/GFDL Ocean Group Tech. Rep. 5, 342 pp.

Hameed, S., and S. Piontkovski, 2004: The dominant influence of the Icelandic Low on the position of the Gulf Stream northwall. *Geophys. Res. Lett.,* **31,** L09303, doi:10.1029/2004GL019561.

Harrison, D. E., 1989: On climatological monthly mean wind stress and wind stress curl fields over the world ocean. *J. Climate,* **2,** 57–70.

Hogg, N. G., 1992: On the transport of the Gulf Stream between Cape Hatteras and the Grand Banks. *Deep-Sea Res.,* **39,** 1231–1246.

——, R. S. Pickart, R. M. Hendry, and W. M. Smethie Jr., 1986: The northern recirculation gyre of the Gulf Stream. *Deep-Sea Res.,* **33,** 1139–1165.

Holland, W. R., and A. D. Hirschman, 1972: A numerical calculation of the circulation in the North Atlantic Ocean. *J. Phys. Oceanogr.,* **2,** 336–354.

Hughes, C. W., and B. A. De Cuevas, 2001: Why western boundary currents in realistic oceans are inviscid: A link between form stress and bottom pressure torques. *J. Phys. Oceanogr.,* **31,** 2871–2885.

Jarvis, R. A., and G. Veronis, 1994: Strong deep recirculations in a two-layer wind-driven ocean. *J. Phys. Oceanogr.,* **24,** 759–776.

Joyce, T. M., C. Deser, and M. A. Spall, 2000: The relation between decadal variability of subtropical mode water and the North Atlantic Oscillation. *J. Climate,* **13,** 2550–2569.

Large, W. G., J. C. McWilliams, and S. C. Doney, 1994: Oceanic vertical mixing: A review and a model with a nonlocal boundary layer parameterization. *Rev. Geophys.,* **32,** 363–403.

Levitus, S., J. I. Antonov, T. P. Boyer, and C. Stephens, 2000: Warming of the world ocean. *Science,* **287,** 2225–2229.

Lindstrom, S. S., and D. R. Watts, 1994: Vertical motion in the Gulf Stream near 68°W. *J. Phys. Oceanogr.,* **24,** 2321–2333.

Liu, W. T., 2002: Progress in scatterometer application. *J. Oceanogr.,* **58,** 121–136.

Ly, L. N., I. C. Kindle, J. D. Thompson, and W. J. Youtsey, 1992: Wind stress analysis over the western tropical equatorial Pacific and North Atlantic Oceans based on ECMWF operational wind products 1985–89. INO Tech. Rep. TR-3, 110 pp.

Mellor, G. L., C. R. Mechoso, and E. Keto, 1982: A diagnostic model of the general circulation of the Atlantic Ocean. *Deep-Sea Res.,* **29,** 1171–1192.

Munk, W., 1950: On the wind-driven ocean circulation. *J. Meteor.,* **7,** 79–93.

Murray, R. J., 1996: Explicit generation of orthogonal grids for ocean models. *J. Comput. Phys.,* **126,** 251–273.

Nurser, A. J. G., and R. G. Williams, 1990: Cooling Parson's model of the separated Gulf Stream. *J. Phys. Oceanogr.,* **20,** 1974–1979.

Özgökman, T. M., E. P. Chassignet, and A. M. Paiva, 1997: Impact of wind forcing, bottom topography, and inertia on midlatitude jet separation in a quasigeostrophic model. *J. Phys. Oceanogr.,* **27,** 2460–2476.

Parsons, A. T., 1969: A two-layer model of Gulf Stream separation. *J. Fluid Mech.,* **39,** 511–528.

Pedlosky, J., 1987: On Parsons' model of the ocean circulation. *J. Phys. Oceanogr.,* **17,** 1571–1582.

Pickart, R. S., and D. R. Watts, 1990: Deep western boundary current variability at Cape Hatteras. *J. Mar. Res.,* **48,** 765–791.

——, and W. M. Smethie, 1993: How does the deep western boundary current cross the Gulf Stream? *J. Phys. Oceanogr.,* **23,** 2602–2616.

Rahmstorf, S., 1993: A fast and complete convection scheme for ocean models. *Ocean Modell.,* **101,** 9–11.

Rhines, P. B., and R. Schopp, 1991: The wind-driven circulation: Quasi-geostrophic simulations and theory for nonsymmetric winds. *J. Phys. Oceanogr.,* **21,** 1438–1469.

Röske, F., 2001: An atlas of surface fluxes based on the ECMWF re-analysis—A climatological dataset to force global ocean general circulation models. Max Planck Institut für Meteorologie Rep. 323, 31 pp.

Rossby, T., 1999: On gyre interactions. *Deep-Sea Res. II,* **46,** 139–164.

Sakimoto, T., 2002: Western boundary current separation caused by a deep countercurrent. *Geophys. Astrophys. Fluid Dyn.,* **96,** 179–199.

Sarkisyan, A. S., and V. F. Ivanov, 1971: The combined effect of baroclinicity and bottom relief as an important factor in the dynamics of ocean currents. *Izv. Acad. Sci. USSR, Atmos. Oceanic Phys. Engl. Transl.,* **1,** 173–188.

Schott, F. A., R. Zantopp, L. Stramma, M. Dengler, J. Fischer, and M. Wibraux, 2004: Circulation and deep-water export at the western exit of the subpolar North Atlantic. *J. Phys. Oceanogr.,* **34,** 817–843.

Semtner, A. J., and R. M. Chervin, 1992: Ocean general circulation from a global eddy-resolving model. *J. Geophys. Res.,* **97,** 5493–5550.

Smith, R. D., M. E. Maltrud, F. O. Bryan, and M. W. Hecht, 2000: Numerical simulation of the North Atlantic Ocean at 1/10°. *J. Phys. Oceanogr.,* **30,** 1532–1561.

Spall, M. A., 1996: Dynamics of the Gulf Stream/deep western boundary current crossover. Part I: Entrainment and recirculation. *J. Phys. Oceanogr.,* **26,** 2152–2168.

Stommel, H., 1948: The westward intensification of wind-driven ocean currents. *Trans. Amer. Geophys. Union,* **29,** 202–206.

Tansley, C. E., and D. P. Marshall, 2000: On the influence of bottom topography and the deep western boundary current on Gulf Stream separation. *J. Mar. Res.,* **58,** 297–325.

Taylor, A. R., and J. A. Stephens, 1998: The North Atlantic oscillation and the latitude of the Gulf Stream. *Tellus,* **50,** 134–142.

Thompson, J. D., and W. J. Schmitz, 1989: A limited area model of the Gulf Stream: Design, initial experiments and model data intercomparison. *J. Phys. Oceanogr.,* **19,** 791–814.

Vallis, G. K., 2006: *Atmospheric and Oceanic Fluid Dynamics: Fundamentals and Large-Scale Circulation*. Cambridge University Press, 745 pp.

Veronis, G., 1966: Wind-driven ocean circulation.–Part 2. Numerical solutions of the nonlinear problem. *Deep-Sea Res.,* **13,** 31–55.

Verron, J., and C. Le Provost, 1991: Response of the eddy-resolving general circulation numerical models to asymmetrical wind forcing. *Dyn. Atmos. Oceans,* **15,** 505–533.

Winton, M., 2000: A reformulated three-layer sea ice model. *J. Atmos. Oceanic Technol.,* **17,** 525–531.

Worthington, L. V., 1976: *On the North Atlantic Circulation*. Vol. 6, *Johns Hopkins Oceanographic Studies,* The Johns Hopkins University Press, 110 pp.

Wunsch, C., and D. Roemmich, 1985: Is the North Atlantic in Sverdrup balance? *J. Phys. Oceanogr.,* **15,** 1876–1880.

Zhang, R., and G. K. Vallis, 2006: Impact of great salinity anomalies on the low-frequency variability of the North Atlantic climate. *J. Climate,* **19,** 470–482.